

A CHANDRA X-RAY STUDY OF THE INTERACTING BINARIES IN THE OLD OPEN CLUSTER NGC 6791

MAUREEN VAN DEN BERG^{1,2}, FRANK VERBUNT^{3,4}, GIANPIERO TAGLIAFERRI⁵, TOMASO BELLONI⁵, LUIGI R. BEDIN⁶, AND IMANTS PLATAIS⁷

¹Astronomical Institute “Anton Pannekoek”, University of Amsterdam, Science Park 904, 1098 XH Amsterdam, The Netherlands

²Harvard-Smithsonian Center for Astrophysics, 60 Garden Street, Cambridge, 02138 MA, USA; maureen@head.cfa.harvard.edu

³Department of Astrophysics/IMAPP, Radboud University Nijmegen, PO Box 9010, 6500 GL Nijmegen, The Netherlands

⁴SRON, Netherlands Institute for Space Research, Sorbonnelaan 2, 3584 CA Utrecht, The Netherlands

⁵INAF/Osservatorio Astronomico di Brera, Via E. Bianchi 46, I-23807 Merate (LC), Italy

⁶INAF/Osservatorio Astronomico di Padova, Vicolo dell’Osservatorio 5, I-35122 Padova, Italy and

⁷Department of Physics and Astronomy, The Johns Hopkins University, Baltimore, MD 21218, USA

Draft version October 23, 2021

ABSTRACT

We present the first X-ray study of NGC 6791, one of the oldest open clusters known (8 Gyr). Our *Chandra* observation is aimed at uncovering the population of close interacting binaries down to $L_X \approx 1 \times 10^{30} \text{ erg s}^{-1}$ (0.3–7 keV). We detect 86 sources within $8'$ of the cluster center, including 59 inside the half-mass radius. We identify twenty sources with proper-motion cluster members, which are a mix of cataclysmic variables (CVs), active binaries (ABs), and binaries containing sub-subgiants. With follow-up optical spectroscopy we confirm the nature of one CV. We discover one new, X-ray variable candidate CV with Balmer and He II emission lines in its optical spectrum; this is the first X-ray–selected CV confirmed in an open cluster. The number of CVs per unit mass is consistent with the field, suggesting that the 3–4 CVs observed in NGC 6791 are primordial. We compare the X-ray properties of NGC 6791 with those of a few old open (NGC 6819, M 67) and globular clusters (47 Tuc, NGC 6397). It is puzzling that the number of ABs brighter than $1 \times 10^{30} \text{ erg s}^{-1}$ normalized by cluster mass is lower in NGC 6791 than in M 67 by a factor ~ 3 –7. CVs, ABs, and sub-subgiants brighter than $1 \times 10^{30} \text{ erg s}^{-1}$ are under-represented per unit mass in the globular clusters compared to the oldest open clusters, and this accounts for the lower total X-ray luminosity per unit mass of the former. This indicates that the net effect of dynamical encounters may be the destruction of even some of the hardest (i.e. X-ray–emitting) binaries.

Subject headings: open clusters and associations: individual (NGC 6791); X-rays: binaries; stars: activity; binaries: close; cataclysmic variables

1. INTRODUCTION

X-ray emission of late-type stars arises in hot gas contained by magnetic loops above the stellar surface. These loops are produced by the interaction of convective motion and differential rotation in the stellar envelope; hence the magnetic activity of a late-type main-sequence star—and with it the X-ray emission—is found to be higher in rapidly rotating stars (see, for example, Pallavicini 1989). As stars age their rotation slows down, and it was a surprise that a *ROSAT* study of the old open cluster M 67 discovered a large number of X-ray sources (Belloni et al. 1993). Comparison with optical observations provided the explanation: in an old cluster stars may rotate rapidly when tidal forces spin them up towards corotation with the binary revolution (Belloni et al. 1998). X-ray studies of old open clusters help in identifying such, otherwise inconspicuous, active binaries (ABs) in which tidal forces are or have been effective, and contribute to the understanding of tidal interaction. Since the typical timescale for tidal interaction rapidly increases with the ratio of the orbital separation to stellar radius (Zahn 1989), only stars in binaries with relatively short periods or relatively large radii experience the effects of tidal locking. X-ray observations of ABs in old clusters thus probe the populations of hard binaries, and the relative number of such systems found in clusters with different properties is an important tool for understanding the effects of the cluster environment on the binary content.

Thanks to prolonged optical studies, e.g. in the WIYN Open Cluster Study (Mathieu 2000), our knowledge of the binary population in clusters is reaching completeness levels which

enable a detailed comparison with theoretical models of the evolution of stellar clusters and of the binary population in them. To explain the large number of blue stragglers observed in M 67 (4 Gyr), the model by Hurley et al. (2005) requires a large initial number of short-period binaries that act as seeds from which blue stragglers are formed. As the simulated hard-binary fraction and period distribution do not evolve much, the close binaries remain abundant throughout the life time of the cluster. Geller & Mathieu (2012) point out that comparison with the observed binaries in the old cluster NGC 188 (6.5 Gyr; Meibom et al. 2009) finds no evidence of such a high fraction of close binaries. The number of clusters studied is still small, as is the number of detailed models, and more study is required before a final verdict on these and other discrepancies (see Geller & Mathieu (2012) for details) can be made.

By now, observations of globular clusters with the *Chandra X-ray Observatory* have uncovered hundreds of faint ($L_X \lesssim 10^{33} \text{ erg s}^{-1}$) close binaries, only part of which have been classified so far. As these binaries are an important driver of the long-term evolution of a cluster, understanding the properties and frequency of the various binary classes is a major goal of investigating (globular) cluster X-ray sources. Sometimes the outcome of a dynamical encounter is a binary or multiple system in a very unusual configuration, and this allows us to study source types that are not, or only rarely, found in the field. Besides ABs, which are the dominant X-ray source class in old open clusters, globular-cluster X-ray sources include cataclysmic variables (CVs), low-mass X-ray binaries

in quiescence (qLMXBs), and milli-second pulsars (MSPs). The correlation of the numbers of qLMXBs and CVs with the stellar encounter frequency reveals the important role that dynamical encounters play in the creation of such binaries (Pooley & Hut 2006; Heinke et al. 2006), but the net balance between formation and destruction is less clear. For a large part this is due to the lack of a reference point that quantifies their number densities in a dynamically inactive environment. Ideally, the comparison should be made against the Galactic field where stellar densities are low, but this is complicated because of the generally limited information on distance and age for stars in the field, and the intrinsic scarcity of sources such as qLMXBs. Old open clusters provide an alternative that is worthwhile to explore, but so far only few have been studied in detail in X-rays. Moreover, it should be kept in mind that dynamical encounters cannot be completely ignored in open clusters. Observational indications for the occurrence of dynamical interactions have come from individual systems whose properties are difficult to explain by binary evolution as it would take place outside a cluster environment (e.g. van den Berg et al. 2001).

In this paper we present the results of the first X-ray observation of NGC 6791, which, at an age of about 8 Gyr, is one of the oldest known open clusters in our Galaxy. Besides the *Chandra* data, we obtained optical spectra to classify candidate optical counterparts to the detected X-ray sources. NGC 6791 has been studied extensively in the optical. The rich body of available literature has proven to be very useful for the classification of our *Chandra* sources, and for separating cluster members from non-members. For the study of interacting binaries it is a promising target: before this work it was known to harbor two of only three spectroscopically-confirmed CVs found in open clusters (Kaluzny et al. 1997), and many optical-variability studies have revealed dozens of close binaries in the field of the NGC 6791 (see de Marchi et al. (2007) and references therein). It is therefore interesting to investigate if the X-ray source content of NGC 6791 is as rich and varied as was found for the few old open clusters studied previously, viz. M 67 (Belloni et al. 1993, 1998; van den Berg et al. 2004) and NGC 188 (Belloni et al. 1998; Gondoin 2005). The cluster lies at a distance of $\sim 4.0\text{--}4.3$ kpc and is reddened by $E(B - V) = 0.09\text{--}0.16$; see e.g. Carraro et al. (2006), Basu et al. (2011), and Brogaard et al. (2011) for recent determinations of the cluster parameters. Throughout the paper we adopt a distance of 4.1 kpc and a constant reddening $E(B - V) = 0.14$, which corresponds to a neutral-hydrogen column density $N_{\text{H}} = 7.8 \times 10^{20} \text{ cm}^{-2}$ (Predehl & Schmitt 1995). The reddening could vary across the area of the cluster (Platais et al. 2011; Brogaard et al. 2012) but the effect is too small to have a significant impact on our results. NGC 6791 stands out in several ways, including its high age and large mass. Remarkably for such an old cluster, the metallicity is higher than solar ($[\text{Fe}/\text{H}] \approx +0.4$).

The X-ray and optical observations and data reduction are described in Sect. 2, followed by the data analysis in Sect. 3. We detected various types of sources in the cluster which are presented in Sect. 4. Our results are discussed in the context of the populations of interacting binaries in star clusters in Sect. 5. We finish with our conclusions in Sect. 6.

2. OBSERVATIONS AND DATA REDUCTION

2.1. X-ray observations

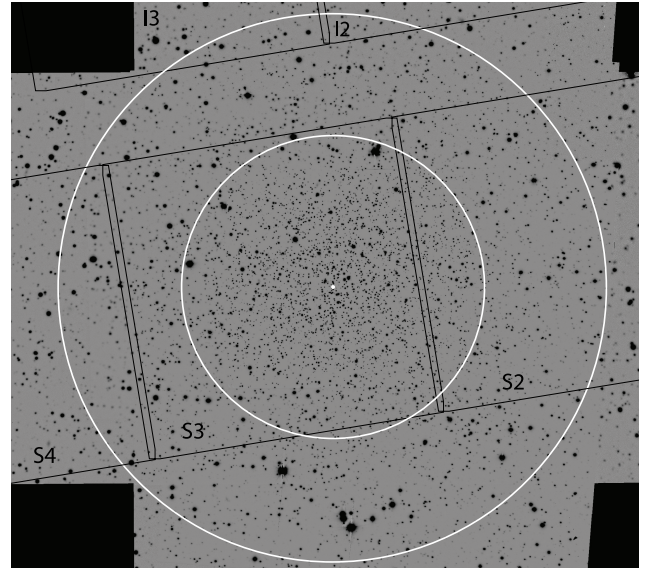


Figure 1. V-band image of NGC 6791 from Stetson et al. (2003) showing in black the outline of the ACIS chips (labelled) as in our *Chandra* observation. The small white, innermost circle indicates the cluster center from de Marchi et al. (2007). The larger white circles mark the area inside the half-mass radius r_h ($4'42''$), and the area inside $8'$, which was analyzed in this paper. North is up, east to the left.

We observed NGC 6791 with the Advanced CCD Imaging Spectrometer (ACIS)¹ on *Chandra* from 2004 July 1 20:51 UTC until July 2 10:49 UTC for a total exposure time of 48.2 ks (ObsID 4510). The observation was done in very faint, timed exposure mode with a single-frame exposure time of 3.2 s. In order to achieve optimal sensitivity below ~ 1 keV, we placed the central part of the cluster on the backside-illuminated S3 chip; the neighboring S1, S2, S4, I2, and I3 chips were used to cover the outer parts of the cluster. The cluster center lies at approximately $\alpha = 19^{\text{h}}20^{\text{m}}53^{\text{s}}$, $\delta = +37^{\circ}46'18''$ (J2000; de Marchi et al. 2007); we shifted the center $0'.5$ away from the S3 aimpoint in the $-Y$ (approximately south-east) direction so that a larger part of the cluster could be imaged on a single chip. Platais et al. (2011) derive a cluster half-mass radius r_h of $4'.42 \pm 0'.02$. Our observation covers almost the entire area inside r_h ($\geq 98.5\%$) with either the S3 or the S2 chip; only the southernmost tip falls off the detector area. Fig. 1 shows the outline of the ACIS chips overlaid on an optical image of the cluster.

Our data reduction started with the level-1 event file produced by version 7.6.7.2 of the *Chandra* X-ray Center processing pipeline. We used the CIAO 3.4 package with the CALDB 3.3.0 calibration files for further processing following standard procedures², including the very-faint mode background cleaning. In order to improve the precision of the source positions we removed the randomization of event coordinates that is applied in standard processing. Towards the end of the observation, the background level between 0.3 and 7.0 keV increased by a factor of ~ 5 as a result of a background flare. After removing this interval from the observation, the exposure time is reduced to 42.9 ks.

2.2. Optical spectroscopy

We obtained low-resolution spectra of candidate optical counterparts to guide the classification of the X-ray sources.

¹ <http://cxc.harvard.edu/proposer/POG/html/ACIS.html>

² http://cxc.cfa.harvard.edu/ciao3.4/guides/acis_data.html

A total of 16 candidate counterparts brighter than $V \approx 18.3$ were observed with the FAST long-slit spectrograph on the 1.5-m Tillinghast telescope on Mt. Hopkins on 9 nights between 2005 June 7 to September 2. We used the 300 lines mm^{-1} grating, resulting in a wavelength coverage from 3480 to 7400 Å and a 3-Å resolution. Exposure time was chosen to achieve a signal-to-noise ratio $S/N \geq 20$ for $V \lesssim 17.5$, and $10 \lesssim S/N \lesssim 20$ for fainter sources. FAST spectra were extracted and wavelength-calibrated with a dedicated reduction pipeline³. Flux standards were observed on the same nights as the science targets.

Candidate optical counterparts fainter than $V \approx 17$ were observed with the fiber-fed multi-object spectrograph Hectospec on the 6.5-m Multi-Mirror Telescope. Use of the 270 lines mm^{-1} grating resulted in spectra that cover 3700 to 9150 Å with a resolution of 6 Å. A total of 16 candidate counterparts were observed on the nights of 2005 May 13 and July 4–6. Each setup was repeated 4 to 5 times with individual exposures of 900 s. Exposures were combined, and the spectra extracted and wavelength-calibrated, with the Hectospec reduction pipeline⁴. Sky background spectra for each setup were created by combining the spectra of fibers positioned at off-source locations. Hectospec observations did not include flux standards. To correct for the instrumental response we constructed sensitivity curves using the spectra of the subdwarf B (sdB) stars B 4, B 5 and B 3 in NGC 6791 (Kaluzny & Udalski 1992), included in the May 13, July 4 and July 5–6 setups, respectively. We assumed that their intrinsic spectra can be described by blackbodies with temperatures as determined for these sdB stars by Liebert et al. (1994). The blackbody spectra were then normalized to reproduce the observed V magnitudes (Stetson et al. 2003) after correction for the cluster reddening. This way we achieved an approximate absolute-flux calibration of the target spectra after applying the resulting sensitivity curves.

Flux-calibrated target spectra were assigned spectral types by comparison to standard spectra with similar resolution (e.g. Jacoby et al. 1984).

3. ANALYSIS

3.1. X-ray source detection and extraction

We restrict the analysis to the area within $8'$ of the cluster center. Sources further away have relatively large positional errors, which complicates the optical identification. We focus on the area inside r_h which is close to the largest circular area around the cluster center that is entirely covered by the observation.

We performed source detection in a broad (0.3–7.0 keV), soft (0.3–2.0 keV) and hard (2.0–7.0 keV) energy band, also used in our *Chandra* study of M 67 (van den Berg et al. 2004), to facilitate comparison. The CIAO detection routine *wavdetect* was run for scales of 1.0 to 11.3 pixels, in steps increasing by a factor $\sqrt{2}$, with the larger scales appropriate for large off-axis angles where the point-spread function (PSF) becomes significantly broader. We computed exposure maps for the response at 1 keV to account for spatial variations of the sensitivity. The *wavdetect* detection threshold was set to 10^{-6} , from which we expect two spurious detections per detection scale (so sixteen spurious detections in total) in the area that we consider here. *Wavdetect* positional errors reflect the sta-

tistical uncertainty in centroiding the spatial distribution of the detected events of a given source, but do not include systematic errors that result from data processing and PSF asymmetries at large offset angles. To compute positional uncertainties we therefore adopt Eq. 5 in Hong et al. (2005). This formula relates the 95% confidence radius on the source position r_{95} to the *wavdetect* counts and offset angle from the aimpoint, and is based on extensive simulated detections of artificial sources. Combination of the broad, soft, and hard-band source lists results in a master catalog of 86 distinct sources within $8'$ of the cluster center, of which 59 lie inside r_h . Table 1 summarizes their basic properties. To investigate the validity of the sources, we also ran *wavdetect* with a threshold of 10^{-7} or an expected number of spurious sources of 1.6. The fourteen sources not detected in this run are marked with an asterisk in Table 1. In this paper we adopt a short version of the source names to refer to the sources instead of using their official CXO names; see columns 1 and 2 in Table 1. The shorthand names are assigned by first sorting the sources within r_h on net counts, and then the sources between r_h and $8'$.

We used the *acis_extract* package (version 3.107.2; Broos et al. 2002) to measure net source counts. Events between 0.3 and 7.0 keV were extracted from a region corresponding to 90% of the PSF at 1.5 keV; for a few sources this region was reduced to avoid contamination by a close neighbor. The background was determined from a source-free annulus centered on the source position. We convert net count rates to fluxes within *Sherpa*⁵ with *arf* and *rmf* response files appropriate for the chip location and source-extraction area of each source. Column 7 of Table 1 lists absorption-corrected (u) fluxes $F_{X,u}$ computed under the assumption that the underlying spectrum is an optically thin plasma (described by the *xsmekal* model) with $kT = 2$ keV. For source CX 29 that lies near the aimpoint 1 count s^{-1} corresponds to 6.8×10^{-12} erg $\text{cm}^{-2} \text{s}^{-1}$. This temperature is appropriate for the most active ABs in the cluster (see e.g. van den Berg et al. 2004), while too high for the least active ABs and too low for most CVs. For a 1-keV *Mekal* model, a power-law spectrum (*powlaw1d*) with photon index $\Gamma = 2$, and a 10-keV thermal-bremsstrahlung model (*xsbremss*) the conversion factor is 24% smaller, and 30% and 42% larger, respectively. In each case we account for a column density equal to the cluster value using the *xsphabs* model. For the adopted distance to NGC 6791 of 4.1 kpc, a 3-count detection limit corresponds to a limiting unabsorbed X-ray luminosity $L_{X,u}$ of $(0.7 - 1.4) \times 10^{30}$ erg $\text{s}^{-1} \text{cm}^{-2}$ (0.3–7 keV) where the range corresponds to the choice of models specified above.

Acis_extract performs a Kolmogorov-Smirnov test on the event arrival times to test for variability. Two sources are thus found to be potentially variable, with probabilities that their count rates are constant (p_{K-S}) smaller than 2.5%: CX 19 (a candidate CV, see Sect. 4.2) for which 15 of a total of 19 counts are detected within 5.5 hours ($p_{K-S} = 0.018$), and CX 37 (no optical counterpart found) for which all 9 counts are detected in the first 7 hours of the observation ($p_{K-S} = 0.024$).

3.2. X-ray spectral properties

Only CX 1 has sufficient counts to allow a constraining spectral fit. A spectrum was extracted from the *acis_extract*

³ <http://tdc-www.harvard.edu/instruments/fast>

⁴ <http://tdc-www.harvard.edu/instruments/hectospec/>

⁵ <http://cxc.harvard.edu/sherpa>

Table 1
Chandra sources within 8' of the center of NGC 6791

(1)	(2)	(3)	(4)	(5)	(6)	(7)	(8)	(9)	(10)
CX	CXOU J	α (J2000) (deg)	δ (J2000) (deg)	r_{95} (")	Offset (')	Counts	$F_{X,u}$ (erg cm ⁻² s ⁻¹)	E_{50} (keV)	Opt
Sources inside the half-mass radius r_h									
1	192044.9+374640	290.187175	+37.777870	0.32	1.64	213 ± 15	318.0	1.3 ± 0.1	+
2	192039.8+374354	290.165914	+37.731752	0.39	3.54	151 ± 13	242.9	1.00 ± 0.03	+
3	192035.7+374452	290.148996	+37.747852	0.39	3.70	125 ± 12	260.1	1.4 ± 0.1	+
4	192056.3+374613	290.234628	+37.770331	0.34	0.66	116 ± 11	170.7	1.4 ± 0.1	+
5	192047.3+374318	290.197161	+37.721768	0.43	3.20	72 ± 9	118.0	1.4 ± 0.1	–
6	192114.4+374530	290.310342	+37.758603	0.63	4.32	72 ± 9	112.0	1.4 ± 0.1	–
7	192052.3+374550	290.218110	+37.764148	0.35	0.47	53 ± 8	77.9	1.2 ± 0.1	+
8	192038.2+374441	290.159518	+37.744838	0.46	3.33	48 ± 7 ^b	221.7	1.6 ± 0.2	+
9	192058.4+375008	290.243732	+37.835590	0.56	3.98	37 ± 7	59.8	1.6 ± 0.3	+
10	192037.3+374612	290.155726	+37.770073	0.43	3.09	34 ± 6	69.3	1.4 ± 0.2	–

Note. — Columns: 1) source number; 2) source name; 3 and 4) source coordinates in decimal degrees after applying the boresight correction of $\Delta\alpha = -0'.06 \pm 0'.06$, $\Delta\delta = -0'.21 \pm 0'.04$ (*Chandra* minus optical); 5) 95% uncertainty radius on the source position; 6) angular offset from the cluster center; 7) net counts in the 0.3–7 keV band; 8) unabsorbed flux ($\times 10^{-16}$ erg s⁻¹ cm⁻²) in the 0.3–7 keV band for the assumption that the source spectrum is a 2-keV Mekeal plasma seen through a neutral-hydrogen column of density 7.8×10^{20} cm⁻²; 9) median energy in the 0.3–7 keV band (only for sources with >5 counts); 10) flag for the detection of a candidate optical counterpart. Table 1 is available in its entirety in a machine-readable form in the online journal. A portion is shown here for guidance regarding its form and content.

source region with the CIAO tool *psextract*, and was grouped to have at least 20 counts bin⁻¹ to warrant use of the χ^2 statistic; the background contribution (<1 count) can be ignored. Given the classification of CX 1 as an active galactic nucleus (AGN) based on its optical spectrum (Sect. 4.6), we try to fit the data with an absorbed power-law and find an acceptable result for a photon index $\Gamma = 1.9 \pm 0.3$ and a column density $N_H < 1.2 \times 10^{21}$ cm⁻² (1- σ upper limit; $\chi^2 = 9.5$, 6 degrees of freedom). The limit on N_H is consistent with the integrated Galactic column density in the direction of NGC 6791 (9×10^{20} cm⁻², Schlegel et al. 1998) while the value for Γ is typical for an AGN (e.g. Tozzi et al. 2006).

The remaining sources have too few counts for useful constraints by spectral fitting. Instead we use the method of quantile analysis developed by Hong et al. (2004), where the median energy (E_{50}) and the 25% and 75% energy quartiles (E_{25} and E_{75}) of the source photons are used to characterize spectral properties. The advantage of using energy quantiles as opposed to comparing counts in pre-defined energy bands by means of hardness ratios is that the errors on the diagnostics are less sensitive to the underlying spectral shape

3.3. Optical identification

3.3.1. Cross-identification against the Stetson catalog

We looked for optical counterparts in the deep *BVI* photometric catalog of NGC 6791 compiled by Stetson et al. (2003; S03 hereafter), which covers the entire area studied here. The limiting magnitude is $V \approx 24$ for the central area but the sensitivity is lower for the outer regions. In an attempt to eliminate artifacts from the catalog, we removed entries with photometric-quality indicators that flag them as suspicious, viz. sources with $|\text{sharpness}| > 1$, and separation index < 0 ; see S03 for an explanation of these indicators and a motivation for these criteria.

We first measure and correct for the boresight, i.e. a possible systematic offset between the astrometric reference frames of the *Chandra* and optical positions. The optical positions are tied to the International Celestial Reference System (ICRS) with an rms accuracy of about 0'.27 (S03), but the as-

tronometric reference frame of any given *Chandra* observation as a whole is aligned to the ICRS with a typical 0'.6 accuracy (90% uncertainty⁶). We measure the boresight correction using matches with optical variables only. This minimizes the number of chance alignments as the light curves of many variables reveal them as close binaries and therefore as plausible X-ray emitters. A list of variables was compiled from the studies of Kaluzny & Rucinski (1993), Rucinski et al. (1996), Mochejska et al. (2002, 2003, 2005), Bruntt et al. (2003), Hartman et al. (2005), and de Marchi et al. (2007); we only selected variables that we could identify with objects in the S03 catalog so that we could use the S03 positions for the boresighting. The boresight correction is computed iteratively. We looked for matches to X-ray sources with more than 10 net counts and $r_{95} \leq 1''$. For each source, the match radius is set to be the quadratic sum of the error on its X-ray position, and the typical 1- σ error on the optical positions (0'.27) scaled to a 95% error radius assuming a 2D gaussian error distribution. The boresight is set to be the weighted (with r_{95}^{-2}) mean of the X-ray–optical offsets of all matches found. Next, the X-ray positions are corrected for the boresight, and the matching is repeated, now including the statistical error on the mean boresight in the match radius. This procedure quickly converges to a boresight correction of $\Delta\alpha = -0'.06 \pm 0'.06$, $\Delta\delta = -0'.21 \pm 0'.04$ (*Chandra* minus optical) based on ten matches with optical variables. Matching the boresight-corrected X-ray catalog to the clean S03 catalog results in 51 optical matches (including 26 variables) for 47 sources, out of the 86 X-ray sources in total.

The probability to find a match in the S03 catalog by chance depends on the projected star density (which decreases with distance from the cluster center r) and on the match radius (which typically increases with r because r_{95} increases). To estimate the expected number of spurious matches, we divide the cluster in a central area defined by $r \leq r_h$, and an outer area of $r_h < r \leq 8'$. The clean S03 catalog gives a projected density of 0.030 optical sources arcsec⁻² and 0.0092 sources

⁶ <http://cxc.harvard.edu/cal/ASPECT/celmon/>

arcsec⁻² for the central and outer area, respectively. If we multiply this by the total area covered by the match circles of the X-ray sources, we find that the expected number of random matches is 5.9 (center), and 3.8 (outer annulus). This amounts to 15% and 29% of the matches found in the respective regions. On the other hand, a similar calculation shows that all matches with variable stars are likely to be real, with the average number of chance alignments < 0.1 both for the central and outer regions.

In order not to overlook any matches, we repeated the matching using the entire S03 catalog, and inspected the regions around the *Chandra* sources in the optical fits image from S03 to discard matches with image artifacts or dubious detections. We thus found nine extra candidate counterparts for eight *Chandra* sources, which are not included in the clean catalog because the values of the quality flags slightly exceeded the adopted cutoff limits, the object is really extended, or because the object is faint and lies close to a relatively bright star. Since selection of these additional counterparts was not done in a very systematic way but relies on visual inspection, it is not trivial to estimate the number of random coincidences among the new matches. Two new candidate counterparts are matched to a single *Chandra* source outside r_h , so at least one of the two must be spurious. The other seven are uniquely matched to seven *Chandra* sources inside r_h . Based on the higher source density in the entire S03 catalog compared to the clean S03 catalog, one would expect to find ~ 1.5 extra spurious matches in the central area. Keeping in mind that some of these optical “sources” are not real, we estimate that at most one or two of the seven new matches inside r_h are spurious.

In total the S03 optical survey provides 60 astrometric matches for 55 sources.

3.3.2. *HST* imaging

Bedin et al. (2006) used *Hubble Space Telescope* (*HST*) multi-epoch imaging with the Wide Field Channel on the Advanced Camera for Surveys (ACS) to measure proper motions of objects in a central $3''.4 \times 3''.4$ region of NGC 6791. We make use of their results to establish cluster membership of candidate counterparts included in the ACS images (Sect. 4.1), and refer to Bedin et al. (2006) for details of the data and the proper-motion analysis. We also use these deep images to look for additional faint candidate counterparts. The data set consists of F606W and F814W images taken on 2003 July 16 and 17 (GO-9815), and on 2005 Jul 13 (GO-10471). An astrometric reference frame was created by combining the GO-9815 F814W images with the STScI *Multidrizzle* software, which removes artifacts like cosmic rays and bad pixels, and corrects for the geometric distortion of ACS images. In order to align the coordinate system to the ICRS, we computed an astrometric solution based on the positions of 273 unsaturated stars from the S03 catalog that could be identified in the stacked image. Fitting for zero point, plate scale, and rotation resulted in a solution where the rms residuals of individual stars are $0''.035$ in right ascension and $0''.032$ in declination; this is negligible compared to the X-ray positional errors. The boresighted X-ray positions and error circles were overlayed on this image, and photometry and proper motions for the astrometric matches were extracted from the source catalog created from the entire *HST* data set. We find seven new candidate counterparts for six X-ray sources. The new matches are all likely extra-galactic, given their proper motion or extended morphology. From the fact that two of

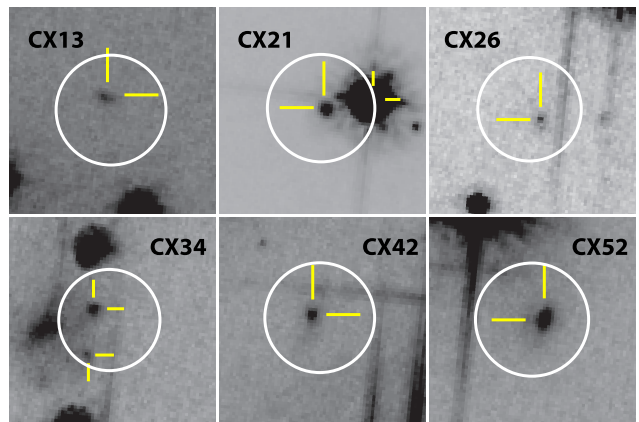


Figure 2. ACS/WFC finding charts, each measuring $3''.4 \times 3''.4$ in size, made from the stacked GO-9815 F814W image representing 7024 s of exposure time in total. The combined X-ray/optical 95% error circles are shown as circles centered around the boresighted X-ray positions, while tick marks indicate the optical matches. Except for the bright candidate counterpart to CX 21 on the edge of the error circle, these matches are found in the *HST* data only, and not in the Stetson et al. (2003) catalog. North is up, east to the left.

the seven *HST* candidate counterparts are matched to *Chandra* sources with another candidate counterpart, we estimate that an appreciable fraction of *HST* matches could be random, on the order of $2/7$ ($\approx 29\%$) or even more. As the astrometrically-calibrated image is not readily available, we show the finding charts of these additional identifications in Fig. 2. This brings the final tally of the optical identification to 53 candidate counterparts for 48 of the 57 X-ray sources inside r_h , and 14 candidate counterparts for 12 of the 29 sources between r_h and $8''$. The properties of the candidate counterparts are summarized in Tables 2 and 3, and their locations in the optical color-magnitude diagrams (CMDs) are shown in Figures 3 and 4. More information on the light-curve properties of the optical variables (column 10 of Table 2) can be found by consulting the original references. Variables with names listed in the format *nnnnn*_* were first discovered by de Marchi et al. (2007); Table 1 in de Marchi et al. (2007) gives an overview of the discovery papers for variables with names starting with a ‘V’ or ‘B’, although updated light curves can sometimes be found in more recent papers mentioned in that table.

3.3.3. Sources with multiple counterparts

For seven X-ray sources we find two candidate counterparts. In four cases—CX 27, CX 57, CX 78, CX 84—one of the two is an optical variable, and given the low probability for a chance coincidence we consider the variables to be the true matches. The variables all lie closer to the X-ray source than the alternative match. We also tentatively list the closest match to the other three X-ray sources as the likely counterpart in Table 2, but more information is needed to firmly establish which, if any, of the two is the true match. For completeness we list the properties of the alternative identifications in Table 3. CX 34 is likely an extra-galactic source, as both *HST* counterparts are extended. The closest match to CX 21 is a faint point source that is unrelated to the cluster; its *HST* proper motion is typical for a background galaxy. The other match is a proper-motion member on the main sequence (see also Fig. 2). CX 82 matches with two bright ($V < 15$) stars. The nearest is a proper-motion non-member and a likely foreground K dwarf.

3.4. Source classification

Table 2
Optical properties of candidate counterparts

(1)	(2)	(3)	(4)	(5)	(6)	(7)	(8)	(9)	(10)	(11)	(12)	(13)	(14)
CX	OID	d_{OX} ($''$)	p_{μ}	V	$B - V$	$V - I$	L_{Xu} ($10^{30} \text{ erg s}^{-1}$)	$\log(F_X/F_V)_0$	Var	P (days)	Optical spectrum	Class	Comments
Proper-motion cluster members													
3	2893	0.23	...	20.64	-0.82	0.63	52.3	-0.06 ± 0.04	B8	CV	...
4	9315	0.09	m	22.70	0.24	0.88	34.3	0.58 ± 0.04	06289.9	...	emission lines	CV	...
9	10050	0.34	99	16.51	1.21	1.22	12.0	-2.35 ± 0.08	early-K giant	RG	...
15	6371	0.16	99	17.27	1.15	1.41	7.7	-2.24 ± 0.09	V9	3.187	early/mid K, filled-in H α	SSG	eclipsing binary
17	12652	0.26	99	17.86	0.27	0.26	6.4	-2.1 ± 0.1	B7	...	Balmer abs. lines with ems. cores	CV	...
22	12695	0.75	99	17.80	0.94	1.02	5.4	-2.2 ± 0.1	V16	2.266	...	AB	eclipsing or spotted binary
23	11111	0.21	98	17.13	0.99	1.07	4.6	-2.5 ± 0.1	V100	12.522	late G/early K	AB	spotted variable?
...	or 23.947	...	late G, filled-in H α ?
30	3626	0.31	99	17.96	1.15	1.29	4.8	-2.8 ± 0.2	V17	6.366	late G, filled-in H α ?	SSG	...
33	10611	1.30	99	19.57	1.04	1.20	3.3	-1.7 ± 0.2	V42	0.506	...	AB	spotted binary
39	5883	0.38	99	17.20	0.89	0.94	2.6	-2.8 ± 0.2	V5	0.313	mid G	AB	contact binary
41	7011	0.23	99	18.27	1.06	1.12	2.3	-2.4 ± 0.2	V76	4.092	late G, early K	SSG	...
44	12390	0.62	99	17.89	0.93	1.01	2.2	-2.5 ± 0.2	V80	4.886	...	AB	eclipsing binary
50	8001	0.28	m	22.72	1.31	2.48	1.7	-0.7 ± 0.2	late K/early M; H α emission	AB	on binary main sequence
54	11278	0.39	96 μ m	19.91	1.07	1.35	1.4	-1.9 ± 0.3	K, filled-in H α	AB?	on binary $V - I$ main seq.
57 ^a	7397	0.20	77	19.27	1.15	1.32	1.1	-2.3 ± 0.3	V41	0.482	...	AB	eclipsing or spotted binary
68	15561	0.92	99 μ m	17.65	...	1.53	12.7	-1.9 ± 0.1	01431.10	7.640	mid K, weak H α emission	SSG	spotted binary
77	746	1.20	99 μ m	17.96	1.35	1.39	4.5	-2.2 ± 0.2	V59	13.833	...	SSG	...
79	13737	0.21	90	21.06	1.45	1.93	2.7	-1.2 ± 0.2	AB	on binary main sequence
81	1185	0.79	99	17.74	0.97	0.96	3.5	-2.4 ± 0.2	V7	0.488	early/mid G	AB	eclipsing binary
86	4773	1.93	99	17.55	1.04	1.03	3.5	-2.5 ± 0.3	V12	1.523	mid G	AB	eclipsing binary
Sources with uncertain or no membership information													
18	6697	0.13	...	23.99	-2.4	1.45	5.9	0.3 ± 0.1	FB	...
19	12116	0.40	...	23.71	0.21	1.30	5.9	0.2 ± 0.1	Balmer and He II emission	CV?	...
25	5627	0.24	...	24.09	0.4	2.12	3.8	0.2 ± 0.1	FB	...
28	10837	0.56	...	22.71	...	0.38	3.8	-0.4 ± 0.2	FB	...
36	6751	0.90	...	20.14	0.53	0.92	3.2	-1.5 ± 0.2	FB	...
49	5910	0.23	45	20.82	1.47	1.79	1.8	-1.5 ± 0.2	mid K, H α emission	AB?	on binary main sequence
56	4436	0.07	...	20.83	1.29	1.69	1.1	-1.7 ± 0.3	01724.9	1.613	...	AB	spotted variable
58	5913	0.35	...	18.38	0.93	0.93	1.1	-2.6 ± 0.3	AB?	on main sequence
65	14602	1.11	...	23.05	-0.4	0.54	9.0	0.1 ± 0.1	00670.10	FB	long-term variable
72	13270	1.31	...	22.9	...	0.5	5.4	-0.1	FB	...

Continued on next page

Table 2
(Continued)

(1) CX	(2) OID	(3) d_{ox} (")	(4) p_{μ}	(5) V	(6) $B - V$	(7) $V - I$	(8) $L_{X,0.3-10}$ ($10^{30} \text{ erg s}^{-1}$)	(9) $\log(F_X/F_V)_{\text{H}}$	(10) Var	(11) P (days)	(12) Optical spectrum	(13) Class	(14) Comments
Sources likely not associated with the cluster													
1	5361	0.19	59	20.36	0.65	0.76	...	-0.09 ± 0.03	AGN, $z \approx 1.16$	EG	...
2	3886	0.14	0	16.22	1.09	1.35	...	-1.86 ± 0.04	V33	1.173	mid K, H α emission	AB	eclipsing binary
7	7878	0.17	0	15.39	1.21	1.49	...	-2.68 ± 0.06	V19	...	late-G, early-K foreground dwarf	S	irregular variable
8	3472	0.17	...	20.22	0.24	0.69	...	-0.30 ± 0.07	AGN, $z \approx 2.36$	EG	...
12	12901	0.92	0	16.06	1.23	1.38	...	-2.65 ± 0.09	V66	50.498	early-K foreground dwarf	S	long-period variable
13	...	0.25	>2.1	EG	extended
21 ^a	...	0.08	nm	23.96	...	1.12	...	0.2 ± 0.1	EG?	proper motion consistent
...	with background galaxy
24	6271	0.29	27	16.32	0.89	1.01	...	-2.9 ± 0.1	V1	0.268	...	AB	foreground contact binary
26	...	0.22	...	28.5	...	1.5	...	1.9 ± 0.2	EG	extended
27 ^a	11376	0.04	0	15.97	0.66	0.81	...	-3.0 ± 0.1	V6	0.279	...	AB	foreground contact binary
29	7328	0.18	0	13.60	0.87	1.26	...	-4.0 ± 0.2	mid K	S	...
31	11212	0.25	...	22.27	0.51	0.75	...	-0.6 ± 0.2	AGN, $z \approx 1.53$	EG	...
34 ^a	...	0.33	>1.6	EG	extended
35	4571	0.28	0	14.62	1.38	1.35	...	-3.7 ± 0.2	mid-K giant	S	...
38	7534	0.12	11, nm	21.04	1.57	2.29	...	-1.2 ± 0.2	S	...
42	...	0.15	...	26.6	...	0.7	...	1.0 ± 0.3	EG	extended
43	3629	0.78	98	22.11	1.75	2.94	...	-0.6 ± 0.2	S	too red to be a member
45	4353	0.37	0	18.98	1.45	1.57	...	-1.7 ± 0.2	$z \approx 0.092$	EG	extended
46	10088	0.21	0	11.54	1.10	1.10	...	-5.1 ± 0.2	mid-G foreground giant	S	...
47	10967	0.32	nm	23.88	-0.2	2.09	...	-0.2 ± 0.2	EG	extended
48	2426	0.66	0	19.53	1.04	1.15	...	-1.8 ± 0.2	V11	0.883	early G	AB	eclipsing binary
51	12037	0.41	0	14.01	0.71	0.74	...	-4.2 ± 0.2	late-F/early-G dwarf	S	...
52	...	0.18	...	27.68	...	2.32	...	1.2 ± 0.3	EG	extended
53	8705	0.20	nm	23.7	0.3	1.3	...	-0.4 ± 0.3	EG	extended
55	...	0.80	...	18.76 ^b	-2.4 ± 0.3	EG?	extended
76	14833	2.37	0	16.48	1.00	1.05	...	-2.9 ± 0.2	V54	8.314	mid-G, early-K foreground dwarf	AB	spotted variable?
78 ^a	553	2.58	0	16.85	1.03	1.10	...	-2.7 ± 0.2	V23	0.272	...	AB	foreground contact binary
80	1031	2.05	0	20.36	0.85	0.94	...	-1.3 ± 0.2	S	...
82 ^a	13404	0.03	0	14.47	0.87	0.89	...	-3.9 ± 0.2	early-K foreground dwarf	S	...
84 ^a	15434	1.49	0	21.2;	...	2.9;	...	-1.2 ± 0.3	01225_10	S	long-term variable

^aThis source has another candidate counterpart, see Table 3.^bThe counterpart is not included in the S03 catalog. The listed value is the magnitude in the g' band (Platais et al. 2011).

Note. — Columns: 1) source number; 2) number of candidate optical counterpart in the S03 catalog, sources without a number were found in the *HST*/ACS images or (for CX 55 only) by visual inspection of the S03 cluster image; 3) angular separation between the X-ray and optical source *after correcting for boresight*; 4) probability for cluster membership, where numeric values are based on the proper-motion studies of Platais et al. (2011) (the case of CX 3 is described in more detail in Sect. 4.2) and K. Cudworth et al. (private communication), and the labels “m” (“members”) and “nm” (“non-members”) are based on the *HST*/ACS study described in Bedin et al. (2006); 5–7) optical magnitudes and colors from S03, except for the (unnumbered) *HST* counterparts where we list the F606W magnitude and the F606W – F814W color if available; 8) unabsorbed X-ray luminosity (0.3–7 keV) in units of $10^{30} \text{ erg s}^{-1}$ assuming a distance of 4.1 kpc and the fluxes in Table 1; 9) ratio of X-ray (0.3–7 keV) to V band fluxes after correcting for extinction; 10) name of the associated optical variable; 11) period of variability; 12) spectroscopic properties of the candidate optical counterpart; 13) source class: CV and CV? = (candidate) cataclysmic variable, AB and AB? = likely or candidate active binary, SSG = sub-subgiant, RG = red giant, S = likely foreground star not associated with the cluster without any indication of binarity, EG = extra-galactic source, FB = Faint object to the Blue of the main sequence; 14) comments. Information on optical variability was gathered from the following references: Kaluzny & Rucinski (1993), Rucinski et al. (1996), Mochejska et al. (2002, 2003, 2005), Bruntt et al. (2003), Hartman et al. (2005), de Marchi et al. (2007), Brogaard et al. (2011)

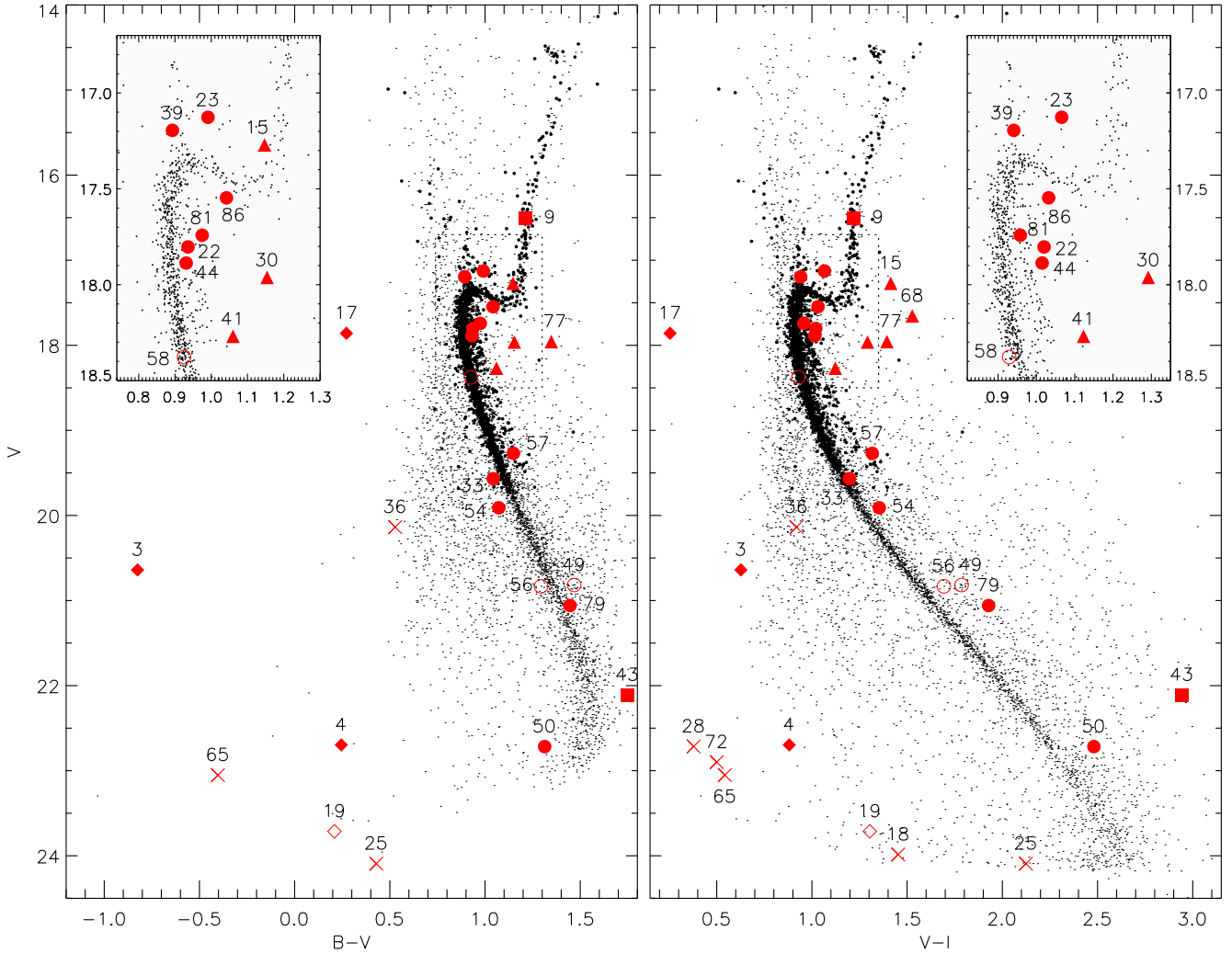


Figure 3. $(V, B - V)$ and $(V, V - I)$ color-magnitude diagrams of NGC 6791 with the candidate optical counterparts that are associated, or possibly associated, with the cluster marked in red. Candidate counterparts that are proper-motion members are indicated with large filled symbols, and sources without membership information with large open symbols or crosses: diamonds are (candidate) CVs, circles are (candidate) ABs, triangles are sub-subgiants, squares are stars without any indication of binarity, and crosses mark unclassified faint sources away from the main sequence. Stars in the field of NGC 6791 are plotted as dots, while stars with a proper-motion membership probability $> 50\%$ (K. Cudworth, private communication) are shown as small filled black circles. The insets zoom in on the crowded regions of the diagrams. Photometry is from Stetson et al. (2003). See the electronic edition of the Journal for a color version of this figure.

Table 3
Alternative optical counterparts

CX	OID	d_{OX} (")	V	$B - V$	$V - I$	comment
21	11098	0.78	18.48	0.93	0.97	$p_{\mu} = 90$
27	11365	0.68	16.58	0.76	0.94	$p_{\mu} = 0$, F star
34	...	0.68	extended
57	7395	0.76	21.02	1.47	1.96	non-member, K star
78	569	3.12	16.50	0.95	1.03	$p_{\mu} = 0$
82	13395	0.70	14.66	0.96	0.98	...
84	15442	3.01	20.64	...	1.7	...

Note. — See Table 2 for the closest astrometric optical match to the X-ray source, and for the meaning of the columns.

Many factors contribute to the classification of the X-ray sources. An extended morphology of the candidate optical counterpart separates extra-galactic from galactic sources. Based on optical spectra one can immediately distinguish between AGN, accreting binaries with substantial accretion disks, and ordinary stars. Period and shape of the optical

light curve constrain the nature and period of a close binary. Proper-motion information, and to some extent optical colors, can establish cluster membership and puts limits on the distance. To distinguish between cluster members and non-members we mainly rely on the proper-motion study by Platais et al. (2011), which includes 41 of our candidate counterparts. For nine additional candidate counterparts membership could be established from the *HST* study by Bedin et al. (2006, see Sect. 3.3.2) and from the results of the proper-motion study by K. Cudworth (private communication).

We use the energy quantiles to constrain the underlying X-ray spectrum for sources with more than 15 net counts (0.3–7 keV). For fainter sources the errors on the quantiles are too large to meaningfully say anything about their spectra. Quantile color-color diagrams (QCCDs) are shown in Fig. 5. Each panel shows two types of model grids, which indicate the expected locations of a source in the QCCD for emission from a Mekal plasma (blue/yellow) and for a power-law spectrum (black/gray). The former is appropriate for the emission from hot coronae around active stars for which the plasma temperature kT can reach up to several keV. CVs can be anywhere

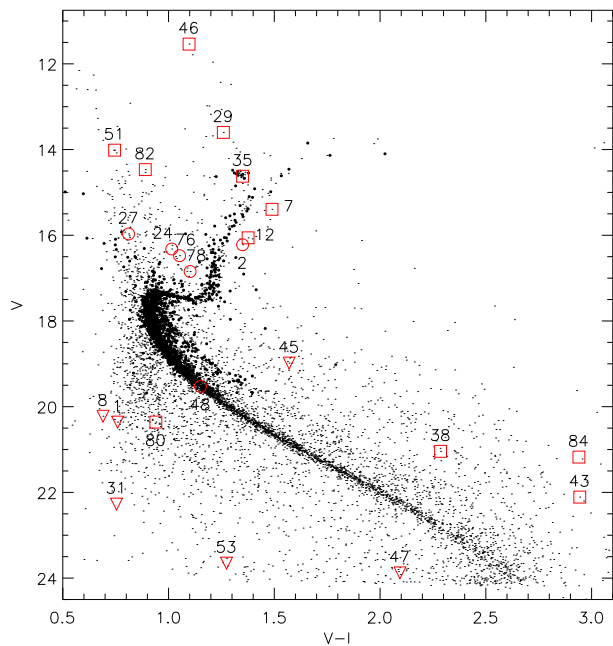


Figure 4. Color-magnitude diagram of NGC 6791 with candidate counterparts that are likely not associated with the cluster marked in red. Downward-pointing triangles are background galaxies, circles are (candidate) ABs, and squares are likely foreground stars without any indication of binarity. *HST* counterparts, for which photometry in *V* and *I* is not available, are not shown. See the electronic edition of the Journal for a color version of this figure.

between soft or very hard; the spectrum of a typical dwarf nova has $kT \approx 2 - 10$ keV (e.g. Byckling et al. 2010). Power-law spectra are appropriate for the harder emission from AGN ($\Gamma = 1 - 2$). Grids are computed with Sherpa using the energy response of the source closest to the aimpoint. Variations in the shape of the grids as function of chip position are typically smaller than the errors on the measurements, and are ignored.

The ratio of the fluxes in the X-ray and optical (*V*) band, or limits thereon, can help to classify a source, even in the absence of an optical match down to the limit of the observations. We compute this ratio as follows: $\log(F_X/F_{\text{opt}})_u = \log(F_X)_u + (V - A_V)/2.5 + 5.44$. The zeropoint for the *V*-band flux is taken from Bessel et al. (1998). The total extinction A_V was assumed to be equal to the cluster value, which underestimates (overestimates) the flux ratio for foreground (background) objects. Typically, stars and active binaries have $\log(F_X/F_V)_u \lesssim -1$, while AGN, CVs or other accreting binaries with unevolved late-type companions, and very active late-type dwarfs can have higher ratios (e.g. Stocke et al. 1991).

4. RESULTS

4.1. Cluster members versus non-members

Twenty candidate counterparts are proper motion members. Of these, all but one (CX 9) show signs of binarity. On this basis we consider at least 19 of them as the true counterparts to the *Chandra* sources. We derive the binary status and type of binary from the optical spectra, the optical light curves, or a location in the CMD on the binary main sequence, indicating that an unresolved multiple system is responsible for the detected light. The cluster binaries are a mix of CVs, ABs, and binaries below the sub-giant branch, and are discussed further in Sects. 4.2, 4.3, and 4.4, respectively. CX 9 is discussed in Sect. 4.5. Cluster members are marked with filled symbols in the CMDs of Fig. 3.

A total of 30 sources are not, or likely not, associated with the cluster. These are stars and binaries with proper motions that clearly set them apart from the members, background galaxies, and stars whose very red colors classify them as unlikely members. They are shown in Fig. 4 and briefly discussed in Sects. 4.5, 4.6, and 4.7.

For ten candidate counterparts membership information is lacking or inconclusive. These sources include (candidate) ABs, a new candidate CV, and faint optical sources that lie to the blue of the main sequence; the latter are discussed in Sect. 4.7. Open symbols and crosses mark them in Fig. 3.

In the following we discuss the sources by type of X-ray emitter. Unless stated otherwise, X-ray luminosities quoted in the text refer to the 0.3–7 keV band.

4.2. Cataclysmic variables

We have detected three CVs that belong to the cluster and discovered one CV candidate without membership information. For all four, the X-ray colors and luminosities are in the expected range for CVs. While the X-ray-to-optical flux ratios in Table 2 are also typical for CVs, their values can be misleading: the X-ray and optical data are not contemporaneous, while CVs may show large variations in brightness on a time scale of weeks to months.

CX 4 is matched to the faint cluster member and optical variable 06289.9 that lies to the blue of the cluster main sequence. Based on its optical colors and the detection of an outburst-like event, de Marchi et al. (2007) already suggested that this star is a dwarf nova. To our knowledge the Hectospec spectrum in Fig. 6, which shows the Balmer lines clearly in emission, is the first spectroscopic confirmation of its CV nature. The X-ray quantiles suggest that the X-ray emission arises in a $kT \approx 4 - 10$ keV plasma (Fig. 5). Thus L_X in Table 2, which was computed for the assumption of a 2-keV plasma, can be up to $\sim 40\%$ too low (see Sect. 3.2).

The new candidate CV is the X-ray variable CX 19, which is matched to a faint blue object with a Hectospec spectrum that shows He II 4686 Å and H β emission lines (Fig. 6), and hints of H α and H δ in emission. The X-ray luminosity ($L_{X,u} \approx 6 \times 10^{30}$ erg s $^{-1}$), the hard spectrum as suggested by its quantile values (Fig. 5), and the high (F_X/F_V) ratio, are all consistent with a classification as CV. He II 4686 Å is of comparable strength as H β . This is seen in high mass-transfer rate systems (nova-like CVs), and in CVs containing white dwarfs with much stronger magnetic fields (i.e. ≥ 1 MG) than in dwarf novae systems. If we assume cluster membership we find an absolute magnitude $M_V \approx 10.2$, which favors the explanation as a magnetic CV.

CX 3 and CX 17 are the known, spectroscopically-confirmed CVs B8 and B7 (Kaluzny et al. 1997). With $L_{X,u} \approx 5.2 \times 10^{31}$ erg s $^{-1}$, B8 is the brightest X-ray source in the cluster. The actual value of L_X is likely higher, as the X-ray quantiles suggest a plasma temperature (~ 4 keV) that is higher than our nominal value. B8 has been classified as a SUUMa dwarf nova based on the detection of several outbursts of 1–2 mag in amplitude, and a recent superoutburst (~ 3 mag) in the Kepler light curve (Mochesjska et al. 2003; Garnavich et al. 2011). We include B8 among the cluster members. Platais et al. (2011) estimated a 10% membership probability from proper motion, but closer inspection of the data reveals that a few detections of this star were contaminated by a fainter close neighbor. When the affected data points are not considered, the proper motion of B8 is consis-

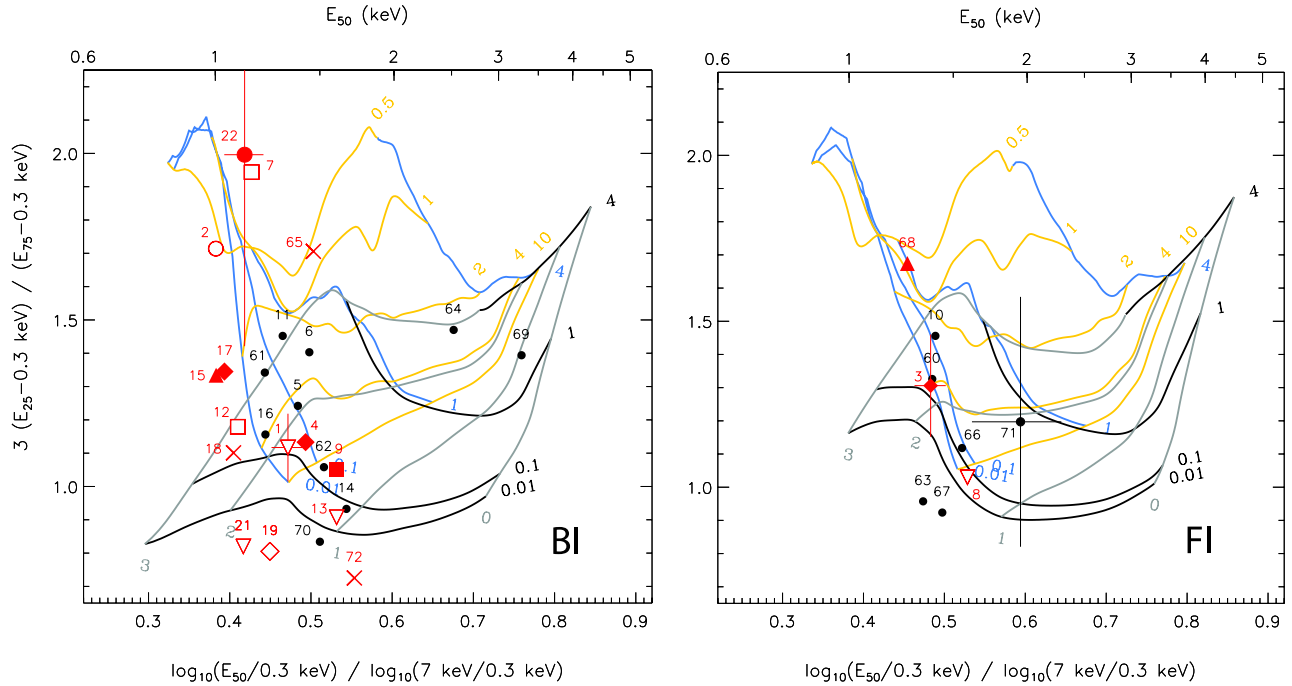


Figure 5. Quantile color-color diagrams with model grids representing a Mekal plasma (blue/yellow) and a power-law spectrum (black/grey). For a certain choice of model, the plasma temperature or spectral index, and the column density can be estimated from the location of a source inside the grid. The median energy E_{50} can be read off from the top x-axis. Symbols are as in Figures 3 and 4, while black filled circles mark sources without optical counterparts. Due to their different energy responses, sources on the background-illuminated (BI) S3 chip and foreground-illuminated (FI) S2 and S4 chips are shown in separate panels. We include sources with more than 15 net counts (0.3–7 keV); error bars are shown only for the sources with the highest and lowest number of counts.

tent with cluster membership.

CX 17 or B7 is a solid cluster member. The X-ray quantiles indicate that $kT \approx 2$ keV. Most reports in the literature find B7 to be relatively bright with $V \approx 18$, which suggests a high mass-transfer rate; occasional small (0.5–1 mag) outbursts, and a drop in brightness of ~ 3 mag in V have also been seen. Mochejska et al. (2003) propose that B7 is a nova-like variable of the VY Scl type, or perhaps a ZCam dwarf nova mostly seen during periods of standstill between minimum and maximum brightness. Our Hectospec spectrum is qualitatively similar to the spectrum in Kaluzny et al. (1997), and likely taken when the mass-transfer rate was high and the disk optically thick: the spectrum shows broad Balmer absorption lines with narrow emission cores, with the emission component dominant in $H\alpha$ (Fig. 6).

The X-ray-to-optical flux ratios and blue optical colors of CX 18, CX 25, CX 28, CX 36, CX 65, and CX 72 resemble those of CVs, and these sources are prime targets for optical follow-up spectroscopy.

4.3. Active binaries

We classify a total of twenty sources as likely or candidate ABs. Thanks to the extensive photometric variability studies of NGC 6791, the orbital periods of many of these can be inferred from the light curves, either through eclipses, ellipsoidal variations, or spot activity. Among the cluster members we find eleven ABs, including eight with photometric periods (Table 2). Most have colors that place them near the main sequence or, in the case of the WUMA contact binary CX 39, right at the turnoff. For CX 86, the 1-sigma errors on $B-V$ and $V-I$ are such that it could lie anywhere from just below the turnoff to the base of the red-giant branch. CX 23 lies securely above the sub-giant branch, and we discuss it separately below. NGC 6791 is at least 8 Gyr old; by comparison to the orbital period versus eccentricity distribution of solar-type spec-

troscopic binaries in the 6.5-Gyr old open cluster NGC 188 it is expected that, for main-sequence binaries, orbits up to at least 15 days have been circularized at the age of NGC 6791 (Mathieu et al. 2004). Therefore, since tidal synchronization operates on a shorter time scale than tidal circularization (Hut 1981; Zahn 1989), main-sequence binaries with periods below 15 days are also expected to be tidally locked. All of our main-sequence ABs with measured photometric periods have periods shorter than 4.9 d; in Sect. 5.2 we discuss how this could be due to the period versus X-ray luminosity relation of ABs and our detection sensitivity. CX 50, CX 54, and CX 79 are not identified with known variables, but they lie on the binary main sequence or have $H\alpha$ in emission in their spectra, which is a signature of enhanced magnetic activity. We note that in the V versus $B-V$ CMD, CX 54 lies slightly to the blue of the main sequence. This is not expected for the combined light of two main-sequence stars, so its classification as AB is less secure. Perhaps this star is a non-member after all, with a proper motion that is similar to that of the cluster stars. Radial-velocity measurements can provide more clarity.

Stars that have evolved past the turnoff, i.e. have evolved to larger radii, can in principle circularize wider orbits than main-sequence stars within a given time span as the circularization time scale is very sensitive to radius. For the sub-giant AB CX 23 the eccentricity is unknown, and estimates of the binary period are only known from photometric variability. Bruntt et al. (2003) quote a period of ~ 12.5 d, while Mochejska et al. (2005) find nearly twice that value, ~ 23.9 d. From the V and $B-V$ measurements of the optical counterpart, we estimate that the radius of the primary is at most $\sim 2.8 R_{\odot}$ (Flower 1996); as both components of the binary likely contribute to the measured optical light, the actual radius of the primary is smaller. If we now look at the diagnostic diagram in Verbunt & Phinney (1995, Fig. 5a; appropriate for a primary mass of $1.25 M_{\odot}$, i.e. somewhat larger than the turnoff

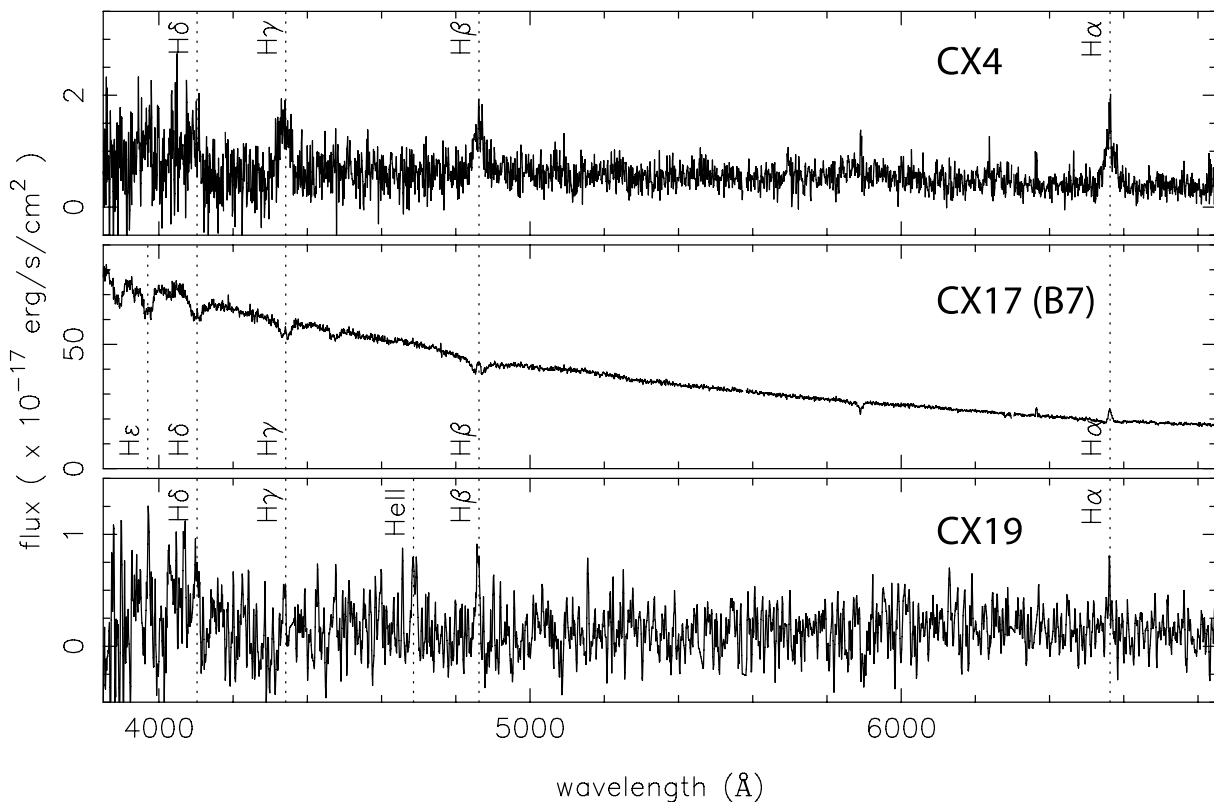


Figure 6. Hectospec spectra of two CVs and one candidate CV. Top: our optical spectrum of CX 4 = 06289.9 confirms this optical variable and cluster member is a CV, as was already suggested by de Marchi et al. (2007). Middle: the spectrum of the known member CV CX 17 = B7 shows narrow emission lines superposed on a continuum with broad Balmer absorption features, indicating a high accretion rate. Bottom: the new candidate CV CX 19. To reduce noise, its spectrum has been smoothed with 3 pixels ($\Delta\lambda \approx 3.6 \text{ \AA}$). Regions where imperfect sky subtraction left large residuals (around 5577 \AA and 6300 \AA) have been removed.

mass in NGC 6791), it is clear that, to first approximation, the primary in CX 23 is too small to have circularized a 23.9-d orbit. This means that in order to explain the X-rays, the rotation of the primary would have to be synchronized to the orbital motion around periastron, assuming the binary was not circular to begin with. However, this leaves the photometric period, which has been tentatively attributed to spot activity and thus reflects the primary’s rotation period, unexplained. The shorter period found by Bruntt et al. (2003) is more consistent with the detection of X-ray activity, as a 12.5 d orbit is short enough for tidal synchronization and circularization to have been achieved. The level of X-ray activity is still unusually high for such a period (Sect. 5.2). With radial-velocity measurements the exact period and eccentricity of the orbit can be verified.

Three candidate counterparts without or with ambiguous membership information are classified as (candidate) ABs near the main sequence. CX 56 is a 1.6-d spotted variable. If CX 49 is a member, it is almost certainly an AB owing to its location on the binary main sequence and H α emission. CX 58, for which we do not have an optical spectrum, lies on the cluster main sequence but could still be an AB in the cluster if the companion is faint.

Six proper-motion non-members are classified as ABs. These include the W UMa contact binaries CX 24, CX 27, and CX 78. The distance modulus inferred from the relation between period, color, and absolute magnitude of contact binaries also place them in front of the cluster (Mochejska et al. 2003).

4.4. Sub-subgiants

Five sources are matched to proper-motion cluster members ($p_m = 99\%$) that stand out due to their optical photometry, which places them below or to the red of the sub-giant branch: CX 15, CX 30, CX 41, CX 68, and CX 77. Stars with similar properties have been labeled “sub-subgiants” or “red stragglers” owing to their unusual location in the CMD, which cannot be explained by the combined light of two ordinary cluster members. About two dozen sub-subgiants are known in open and globular clusters. Various mechanisms (past or ongoing mass transfer, dynamical encounters) have been suggested to explain their photometry but most systems still defy explanation.

All five X-ray detected sub-subgiants in NGC 6791 are optical variables with periods between 3.2 and 13.8 d, and their puzzling photometry has been pointed out before (Kaluzny 2003; Platais et al. 2011). CX 15 is matched to the eclipsing binary V9. Its striking light curve shows smooth, asymmetric brightness modulations that migrate in phase on a time scale of months; these have been attributed to large star spots, and indicate a high level of activity (see for example Mochejska et al. 2005). The other four systems show a single maximum and minimum in the light curve when folded on the periods cited in Table 2, and have been classified as plausible rotational spotted variables (Mochejska et al. 2002; Kaluzny 2003; de Marchi et al. 2007); unambiguous proof of their binarity and orbital periods requires radial-velocity follow-up. While the photometry of CX 41 can be accounted for by the light of three stars—in a bound multiple system or aligned by chance—the red colors of the other four require at least one anomalous star like an underluminous (sub)giant or an overluminous main sequence star. Their detection as X-ray sources

indicates ongoing interaction between companions in a close binary. The weak $H\alpha$ emission in the optical spectra, and the relatively soft X-ray colors are more in line with coronal activity than with an accretion origin of the X-rays. Two more sub-subgiants in NGC 6791 were pointed out by Platais et al. (2011). Star 13753 from S03 falls outside the *Chandra* field. Star 83 is not detected but it lies almost $9'$ from the observation aimpoint so was observed with low sensitivity.

4.5. Stars without indications of binarity

CX9 matches with an early-K giant and cluster member. Our optical spectrum shows no indications of activity, nor is this star known to be an optical variable. Its X-ray colors are unusually hard for a coronal source (Fig. 5). This giant is an interesting target for follow-up studies to investigate if it is a symbiotic-like interacting binary, in which the X-rays are powered by accretion. Alternatively, a faint quasar could be hidden under the point-spread function of this bright star, so a possible explanation is that the giant is a spurious match.

Proper motions exclude cluster membership for the candidate counterparts to CX 7, CX 12, CX 29, CX 35, CX 38, CX 46, CX 51, CX 80, CX 82, and CX 84. These sources are plausible late-type field stars. The proposed counterparts for CX 7, CX 12, and CX 84 are reported to be long-term or irregular variables, but the light curves do not point at binarity; the remaining stars are not known to be variables. Our FAST spectra indicate that CX 35 and CX 46 are (sub)giants. Our assessment of luminosity class is mainly based on the absence or presence of the CN 4216 Å bandhead (Gray & Corbally 2009). The $\log(F_X/F_V)_u$ values, and the soft X-ray colors of CX 7 and CX 12 agree with a coronal origin of the X-rays.

The colors of the faint source CX 43 place it about 0.8 to the red of the lower main sequence and make it an unlikely cluster member. On the other hand, its proper motion is consistent with that of cluster stars. A radial-velocity based membership constraint can provide a more definite answer. Based on the red colors and high $\log(F_X/F_V)_u$ ratio, we suggest this source is a very active late-type star.

4.6. Background galaxies

We classify twelve sources as extra-galactic on various grounds. The optical spectra of CX 1, CX 8, and CX 31 have broad emission lines typical for AGN, and we estimate the redshift z (see Table 2) by comparison with the quasar composite spectrum from Vanden Berk et al. (2001). The counterpart to CX 45 has a redshifted stellar absorption-line spectrum and clearly is extended, even in the ground-based image from S03. The proper motion of the faint unresolved counterpart of CX 21 is consistent with those of background galaxies in the field (Bedin et al. 2006), but we note this source has a bright alternative counterpart on the edge of the error circle that is a cluster member (Sect. 3.3.3). CX 13, CX 26, CX 34, CX 42, CX 47, CX 52, and CX 53 look extended in the ACS images.

Apart from CX 13 and CX 34, which are too faint to get reliable optical photometry for, the extra-galactic sources lie away from the cluster main sequence and most have $\log(F_X/F_V)_u \gtrsim -0.6$. We note that the value of N_H used to calculate this ratio can be underestimated (and the flux ratio therefore overestimated) since extra-galactic sources can have significant intrinsic absorption.

4.7. Uncertain classifications and unidentified sources

Six sources are matched to faint, blue objects without membership information: CX 18, CX 25, CX 28, CX 36, CX 65,

and CX 72. As mentioned in Sect. 4.2, their optical colors and X-ray-to-optical flux ratios are compatible with those of CVs or other accreting binaries with low-mass companions, but also with AGN. Follow-up spectroscopy is needed to further investigate their classification.

A total of 27 sources remain without candidate optical counterparts. For these sources we estimate a lower limit on the X-ray-to-optical flux ratio by assuming $V \gtrsim 24$ (i.e. the limit of the S03 catalog), which gives $\log(F_X/F_V)_u \gtrsim -0.9$. This excludes a stellar coronal origin unless they are very active (flaring) K or M dwarfs, but leaves open the possibility of accreting compact binaries. An extra-galactic nature is the most likely option based on the expected number of AGNs. We compute this number using the cumulative source density versus flux ($\log N - \log S$) curves from Kim et al. (2007), which are derived from *Chandra* pointings at high Galactic latitudes. We assume a 3-count detection limit for the region within $3'$ from the aimpoint, a 5-count limit for larger offsets, and an intrinsic power-law spectrum with photon index $\Gamma = 1.7$ that is absorbed by the integrated Galactic column density in the direction of the cluster ($9 \times 10^{20} \text{ cm}^{-2}$). This predicts ~ 56 AGN. For comparison, we detect 12 galaxies. This suggests that most of the unclassified and unidentified sources (33 in total) are AGN.

5. DISCUSSION

5.1. Cataclysmic variables in NGC 6791

NGC 6791 is the open cluster where most CVs have been found so far. This may not be surprising because, of the open clusters that are old enough to find close binaries in a phase where they can be observed as CVs, NGC 6791 is the most massive one. We check if primordial binaries can account for all observed systems, which comprise the three members (the dwarf novae B8 and CX 4, and the nova-like variable or dwarf nova B7) and the new (possibly magnetic) CV candidate CX 19. Recent observational estimates of the CV number density in the local field differ by a factor of a few but are consistent within the (appreciable) errors: $4_{-2}^{+6} \times 10^{-6} \text{ pc}^{-3}$ (Pretorius & Knigge 2012, non-magnetic CVs only), $0.9_{-0.5}^{+1.5} \times 10^{-5} \text{ pc}^{-3}$ (Rogel et al. 2008), $\sim 1 \times 10^{-5} \text{ pc}^{-3}$ (Grindlay et al. 2005). Adopting the local stellar mass density of $0.045 M_\odot \text{ pc}^{-3}$ from Robin et al. (2003), and scaling the resulting number of field CVs per unit mass to the cluster mass ($\sim 5000\text{--}7000 M_\odot$, see Sect. 5.4), we expect 0.2–3.7 CVs in the cluster. Therefore the observed number of CVs in NGC 6791 is consistent with a primordial population and does not require any dynamical formation or destruction processes.

It is possible that there are more CVs in NGC 6791 that we missed because they are too faint in either X-rays or the optical. Byckling et al. (2010) studied a sample of twelve dwarf novae within $\sim 200 \text{ pc}$ with parallax distances. Only two (GW Lib and WZ Sge) have X-ray luminosities very close or below our detection limit, which is $\sim 1 \times 10^{30} \text{ erg s}^{-1}$ (0.3–7 keV) for the typically hard spectra of CVs. To our knowledge, there are no similar, published, studies of the X-ray luminosity function for magnetic CVs. Systems with moderate magnetic-field strengths (between 1–10 MG, the so-called intermediate polars) are thought to be generally brighter in X-rays than dwarf novae due to the higher mass-accretion rates; see e.g. Heinke et al. (2008). Polars ($B \gtrsim 10 \text{ MG}$) on the other hand can be faint when in the low state with $L_{X,u} \approx 10^{29} - 10^{30} \text{ erg s}^{-1}$. EU Cnc, the CV in M67 (van den Berg et al. 2004), and EF Eri (Schwope et al. 2007) are

two such cases. While polars make up a relatively small fraction of known CVs (about 14% in the catalog by Ritter & Kolb (2003)), their intrinsic contribution to less-biased CV samples is not well known. We estimate that a small ($\sim 15\%$) fraction of dwarf novae and an unknown fraction of polars could have gone undetected by our *Chandra* observation.

The detection limit of the S03 catalog is $V \approx 24$, which corresponds to $M_V \approx 10.5$ at the distance of NGC 6791, taking into account extinction. We compiled a sample of 27 CVs with parallax distances from Patterson et al. (2008), Thorstensen (2003), Harrison et al. (2004), and Thorstensen et al. (2008). Using the typical magnitude of each system (MAG1 in Ritter & Kolb (2003)), we find that the corresponding M_V distribution extends down to $M_V \approx 12.2$, with about 25% of sources (including the X-ray faint systems GW Lib and WZ Sge) below the S03 detection limit.

While the above arguments suggest that we should have detected most CVs in NGC 6791, Gänsicke et al. (2009) found that the period distribution of Sloan Digitized Sky Survey CVs has a spike around the period minimum (80–86 min) corresponding to low-accretion rate systems. The incompleteness of our observations to such faint systems, which have an average magnitude of $M_g = 11.6 \pm 0.7$, is significant.

5.2. Active binaries in NGC 6791

For ABs inside the half-mass radius of NGC 6791, the *Chandra* observation has a detection limit of about $(0.7 - 1) \times 10^{30} \text{ erg s}^{-1}$ (0.3–7 keV) if their coronal temperatures are between 1 and 2 keV. By comparison to the luminosity distribution of ABs in M 67, this implies that many more ABs can be present in NGC 6791 than those listed in Table 2.

Fig. 7 shows the L_X versus orbital-period distribution for ABs in M 67 and NGC 6791. The data for M 67 (open circles) were taken from van den Berg et al. (2004), but, for easier comparison with the present analysis, the X-ray fluxes were recomputed such that they correspond to emission from a 2-keV plasma. The ABs in M 67 show a dominant trend of decreasing L_X with increasing period for orbital periods between about 4–5 and 10 days. This can be explained by the activity-rotation relationship: stars in tidally-synchronized binaries with longer orbital periods rotate slower, and therefore are less active in X-rays, than stars in systems with shorter periods. For the shortest-period ABs, L_X goes down again, which is a result of saturated activity levels. The X-ray luminosity of coronally-active stars does not exceed 0.001 times the bolometric luminosity (e.g. Güdel (2004)), which goes down for the shortest-period binaries. For contact binaries, the maximum X-ray luminosity is even lower, an effect known as super-saturation. In Fig. 7, stars that have evolved past the main-sequence turnoff or that are at the turnoff are plotted with larger symbols. In both clusters, these particular stars are only moderately evolved, with estimated radii no larger than $\sim 3 R_\odot$ (Flower 1996), and all lie on or near the sub-giant branch. Except for two cases, the sub-giant ABs do not show a different trend than the main-sequence ABs (small symbols). The exceptions CX 23 (V 100) in NGC 6791 and S 999 in M 67 (upper right in Fig. 7) lie above the overall rotation-activity trend, and are good targets for follow-up study.

The ABs in M 67 show a clear separation in orbital periods between detections and non-detections (not shown in Fig. 7, but see van den Berg et al. (2004)): practically all binaries with periods below the tidal-circularization cutoff period (12 d in M 67, Latham et al. 1992) are detected and, except for eccentric systems with pseudo-synchronous ro-

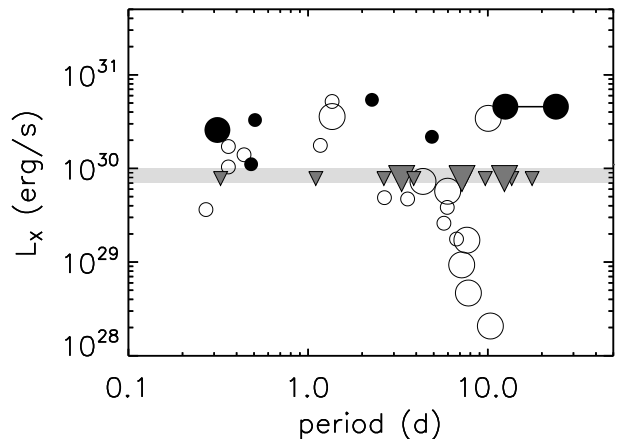


Figure 7. L_X versus orbital-period distribution of ABs inside the half-mass radii of M 67 and NGC 6791. Small symbols are systems on the main-sequence, larger symbols mark systems at the turnoff or on the sub-giant branch. The eccentric binaries S 1242 and S 1272 in M 67 are plotted at their pseudo-synchronous rotation periods. The two possible periods for CX 23 (Sect. 4.3) are connected with a horizontal line. Our sample of ABs in NGC 6791 (filled circles) is expected to be most incomplete for periods between a few days up to the circularization cutoff period, which agrees with the periods of the undetected periodic photometric variables in the cluster (filled triangles). The shaded area marks the upper limit for detection in NGC 6791. We have used the recent proper-motion membership study from Yadav et al. (2008) to re-assess membership for the M 67 *Chandra* sources and thus classified three more ABs with known periods as likely cluster members; these are CX 15, CX 58 and CX 61 (see Tables 2 and 3 in van den Berg et al. (2004)).

tation periods shorter than 12 d, all normal main-sequence and (sub)giant binaries with longer periods remain undetected down to $L_X \approx (2 - 6) \times 10^{28} \text{ erg s}^{-1}$. This can be understood if the activity levels of the stars in these wider systems are closer to those of single stars in the cluster because their rotation is not (sufficiently) enhanced by tidal coupling. If the ABs in NGC 6791 from Table 2 show a similar trend as those in M 67, it is clear from Fig. 7 that our *Chandra* observation of NGC 6791 can only see the brightest part of the AB population, and that our AB sample is most incomplete for periods ranging from a few days up to the circularization cutoff period in NGC 6791, which is at least 15 d. This is consistent with the period distribution of the detected ABs (filled circles) and non-detected periodic photometric variables with membership probability $p_\mu > 50\%$ (filled triangles at the upper limit of detection in Fig. 7). Variables for which the period is ambiguous are excluded from the figure, and so is the periodic variable V 78 which is more likely to be a pulsator rather than a binary (Kaluzny 2003). Not all ABs are necessarily photometrically variable all the time; a comprehensive radial-velocity survey or deeper X-ray data would be useful to uncover more of them.

5.3. On the origin of sub-subgiants

Sub-subgiants in star clusters are typically detected in X-rays, but the X-ray emission is explained by distinctly different types of binary interaction, making it a rather inhomogeneous group. Some resemble ABs (see Mathieu et al. (2003) for M 67, and Albrow et al. (2001) and Heinke et al. (2005) for 47 Tuc), others are CVs (AKO 9 and PC1-V11 in 47 Tuc, Albrow et al. 2001), and at least one but possibly two (in NGC 6397) are in binary MSPs where the X-rays originate in the shock region between the mass outflow from the secondary and the energetic pulsar wind (Bogdanov et al. 2010). The disturbance of hydrostatic equilibrium in the donor in response to mass transfer could explain the CMD location for

the CVs, but the sub-subgiants in M 67 and NGC 6791 show no hint of ongoing mass transfer. Moreover, as has been noted by Mathieu et al. (2003), the eccentric orbit of S 1063 argues against mass transfer in the past, as a (nearly) Roche-lobe filling star would have quickly circularized the orbit on a time scale of $\sim 10^5$ yr. The fact that we see at least five sub-subgiants in NGC 6791 is an argument against invoking *any* short-lived perturbed state (resulting from either regular binary evolution or dynamical encounters with other cluster stars), and is more suggestive of a hitherto overlooked binary evolutionary path. N-body simulations of M 67 by Hurley et al. (2005) created one star below the subgiant branch that offers a possible clue. This simulated star formed when two stars in a binary merged after the donor ascended the sub-giant branch which resulted in a common-envelope phase. The merger product is a single giant with an undermassive core, which explains its location below the normal cluster sub-giant branch. If this scenario applies to the observed sub-subgiants, which all show signs of binarity, the systems should originally be in triples. No primordial triples were included in the models by Hurley et al. (2005), but understanding the origin of sub-subgiants would be a strong motivation for taking them into consideration in future cluster simulations. As has been discussed in the context of blue stragglers by Perets & Fabrycky (2009), triples can indeed facilitate the formation of very close inner binaries that eventually merge or enter a phase of mass transfer.

5.4. X-ray source populations of old open clusters

We compare the close-binary populations in three old open clusters—NGC 6791, M 67, NGC 6819—as probed by X-ray observations to look for trends with cluster properties, specifically mass or age. NGC 6819 was recently studied in X-rays by Gosnell et al. (2012) using *XMM-Newton* data. As we discuss in more detail below, compared to M 67 and NGC 6791, classification of the X-ray sources in the field of NGC 6819 is far less complete at this point, but we include the cluster as it extends the age range of the sample down to 2.4 Gyr. Previous studies have shown that all three clusters have a high fraction of binaries: almost 40% in NGC 6819 (spectroscopic solar-type binaries; Mathieu 2008), $\sim 50\%$ in M 67, and $\geq 25\text{--}30\%$ in NGC 6791 (photometric estimates from the width of the main sequence; Fan et al. 1996 and Bedin et al. 2008). In order to set a uniform sensitivity, we only consider X-ray sources brighter than $L_X = 1 \times 10^{30} \text{ erg s}^{-1}$. We do not include clusters that have been observed with *ROSAT* only (see Belloni (1997) for an overview) as these observations are generally shallower, and the larger positional uncertainties result in less secure source identifications.

Table 4 gives an overview of the cluster properties and the number of X-ray sources N_X , in total and separated by class, detected within the approximate half-mass radii. For NGC 6791 we refer to the list of sources (members and possible members) in Table 2. Platais et al. (2011) estimate a lower limit to the cluster mass of $\sim 5000 M_\odot$; taking into account detection incompleteness, stellar remnants, and binarity, the total mass is likely not higher than $\sim 7000 M_\odot$. For M 67 we adopt a total mass of $\sim 1100 M_\odot$ (Richer et al. 1998). Fan et al. (1996) measured the half-mass radii for several types of stars (giants, single main-sequence stars, and main-sequence binaries); as a result of the effects of mass segregation, they find values ranging from ~ 7.2 to $12'$, depending on the typical mass of the objects. For simplicity, we count the number of *Chandra* sources inside the ACIS-I field (16.8×16.8),

which is close to the area inside any of the r_h estimates by Fan et al. (1996). For both M 67 and NGC 6791 we do not count unidentified sources, or unclassified sources with candidate counterparts that lie away from the main sequence, as possible members because the extra-galactic $\log N - \log S$ curves suggest they are most likely background AGN.

Gosnell et al. (2012) detect twelve sources inside $r_h = 3.3$ down to $L_X = 1 \times 10^{30} \text{ erg s}^{-1}$ (0.2–10 keV) in a *XMM-Newton* pointing of NGC 6819. The estimated number of background sources suggests at most six to seven of these are cluster members. The five sources with candidate optical/UV counterparts include potentially interesting systems like a candidate CV, a candidate qLMXB (the nature of both need to be confirmed spectroscopically), a possible sub-subgiant (X 9), and an RS CVn binary that may have been formed in a dynamical encounter (X 6). Given the depth of the optical catalog ($V \approx 24$) used to look for matches, it is reasonable to assume that an upper limit to the number of cluster ABs is the number of sources with a candidate counterpart on the (binary) main sequence or (sub-)giant branch that cannot be excluded as a non-member. There is at most one such system (X 6). Due to the incomplete source classifications, the total cluster X-ray luminosity is highly uncertain, and we do not list it in Table 4. If we simply take the sum of the luminosities of the twelve sources and divide it by two, we find $\log(2L_{30}/M) \approx 29.1$ (0.2–10 keV); as this estimate is already very approximate, we do not attempt to convert this value to the 0.3–7 keV band. Kalirai et al. (2001) estimate the mass of NGC 6819 to be $\sim 2600 M_\odot$.

The numbers of CVs ($N_{X,CV}$) and sub-subgiants ($N_{X,S}$) are small⁷; only in NGC 6791 are there any spectroscopically confirmed CVs above our luminosity cutoff. A positive correlation of $N_{X,CV}$ and $N_{X,S}$ with cluster mass is allowed. Based on a comparison with the field CV space density, we already argued in Sect. 5.1 that the CVs in NGC 6791 could be primordial, and the same is true for the (candidate) CVs in M 67 and NGC 6819. This indeed implies that $N_{X,CV}$ is proportional to cluster mass.

The value of $N_{X,AB}$ in Table 4 gives the number of normal ABs, i.e. it does not include blue-straggler systems, which may have a non-standard evolutionary history, or the long-period AB-like sources (such as the yellow stragglers S 1040 and S 1072 in M 67; van den Berg et al. 2004). Comparison of $N_{X,AB}$ for the three clusters shows that a simple scaling with the present-day cluster mass is excluded. This is true for the ABs with evolved components ($N_{X,AB-G}$), which have wider orbits and may thus be easier involved in dynamical interactions, but also for ABs on the main sequence ($N_{X,AB-MS}$). Although NGC 6791 is 4.5–6.4 times more massive than M 67, it has 0.9–1.6 times the number of ABs. NGC 6819 has 2.4 times the mass of M 67, but only has a fraction (~ 0.13) of the number of ABs. These ratios show that $N_{X,AB}$ normalized by cluster mass does not show a trend with age or mass either. M 67 has the highest specific AB abundance (~ 0.014 per half the cluster mass), while this number is at least ~ 3 times lower in NGC 6819 and NGC 6791, which are both more massive than M 67, but younger and older, respectively.

It is unclear if the relative dearth of ABs in NGC 6819 and

⁷ The CV EU Cnc in M 67 is fainter in X-rays, and strictly speaking it has not been demonstrated that it is a cluster member. The well-studied sub-subgiant S 1113 in M 67 is not counted in Table 4 as it lies $13.7'$ away from the cluster center. Likewise, the sub-subgiants CX 68 and CX 77 in NGC 6791 lie at $r > r_h$.

NGC 6791 with respect to M 67 can be explained by stellar or binary-evolution arguments, or if cluster dynamics plays a role. Possibly, M 67 is an outlier. Several studies have found that this cluster is dynamically highly evolved (e.g. Davenport & Sandquist 2010). If, as a result of mass segregation, it lost a significant fraction of its mass due to the evaporation of preferentially low-mass stars, the current binary population would appear as representative of a much more massive cluster. To explain the discrepancy in the number of ABs, this effect should be more significant for M 67 than for NGC 6819 and NGC 6791. Another difference is that the X-ray source population of M 67 contains binaries (blue and yellow stragglers) with periods in excess of hundreds of days that look like coronal emitters (but note that these are not included in $N_{X,AB}$ in Table 4); such puzzling systems are not seen in the other two clusters. Clearly, a larger cluster sample spanning wider ranges in age and mass needs to be studied to make sense of what is the norm and what the exception, and understand the X-ray emission of old open clusters (to which ABs contribute an appreciable fraction⁸) in general. As NGC 6791 is one of the oldest open clusters known, we expand our comparison to globular clusters in the next section.

There are two more old (≥ 2 Gyr) open clusters that have been observed in X-rays, but that we have not considered here. The young (1.7–2 Gyr) and nearby cluster NGC 752 is spatially extended with members spread over a much larger region ($\sim 90'$ in diameter) than covered by the *Chandra* and *XMM-Newton* pointings. The census of X-ray sources could thus be very incomplete. We note that the list of detected members from Giardino et al. (2008) includes just one source with $L_X \geq 1 \times 10^{30}$ erg s⁻¹, which is matched to a likely main-sequence AB. Gondoin (2005) analyzed *XMM-Newton* data of NGC 188 with a sensitivity of $L_X = 9 \times 10^{29}$ erg s⁻¹ (0.5–2 keV), about six times deeper than the ROSAT study by Belloni et al. (1998). However, the chosen aimpoint is offset from the cluster center by almost $6'$. Only new observations can tell whether this explains why no sources are detected in 1/4–1/3 of the contiguous area inside the half-mass radius that is farthest from the observation aimpoint. In any case, this unfortunate circumstance makes NGC 188 less suitable to be included in our comparison.⁹

5.5. Comparison with globular clusters

While almost 80 globular clusters have been studied with *Chandra*, only a handful have been observed deep enough to uncover a significant fraction of the ABs. Here we focus on two globular clusters for which the *Chandra* sensitivity reaches well below the luminosity cutoff adopted in the previous section. The nearby core-collapsed cluster NGC 6397 was observed down to a limiting luminosity of $\sim 9 \times 10^{28}$ erg s⁻¹ (Bogdanov et al. 2010). We adopt a cluster mass of $2.5 \times 10^5 M_\odot$ (Pryor & Meylan 1993). Cohn et al. (2010) classified most of the 79 *Chandra* sources inside $r_h = 2'.33$ from Bogdanov et al. (2010) using *HST* data, and found numerous CVs

and ABs, and two sub-subgiants (at least one is in a binary with a MSP). About 20% of the sources are brighter than our cutoff value; these are mostly CVs or neutron-star binaries. While there are plenty of X-ray faint ABs, there are just a few at most above 1×10^{30} erg s⁻¹; the range listed in Table 4 is zero to two, but those two systems have very red colors and are unlikely cluster members. 47 Tuc is a massive cluster ($1.3 \times 10^6 M_\odot$; Pryor & Meylan 1993). We estimate that within $r_h = 2'.79$, about 28 of the 232 sources bright enough to be included in our selection are background AGN, leaving ~ 200 sources associated with the cluster. As of yet, only part of these have been classified (Edmonds et al. 2003a,b). We make a very conservative estimate of the number of CVs and ABs. A lower limit is derived by counting the number of (candidate) CVs and ABs in Table 2 of Heinke et al. (2005), while an upper limit (given in square brackets in Table 4) is estimated by adding all unidentified and unclassified sources to either the CVs or ABs and subtracting the estimated contribution from AGN. Sub-subgiants are more conspicuous, so their number is less uncertain. To compute the cluster X-ray luminosity, we sum the luminosities for the N_X individual sources, and subtract an approximate contribution for the background AGN based on the mean luminosity of the unidentified sources. For both clusters we converted the fluxes listed in Bogdanov et al. (2010) and Heinke et al. (2005) to the 0.3–7 keV band using PIMMS, adopting a 2-keV plasma model.

Table 4 readily shows that the total number of ABs above $L_X = 1 \times 10^{30}$ erg s⁻¹, normalized by cluster mass, is much lower in the two globular clusters than in M 67 and NGC 6791. For 47 Tuc the difference is a factor of 65–230 compared to M 67, whereas NGC 6397 likely does not have any ABs at all above this luminosity. Lowering the X-ray luminosity cutoff value would increase the numbers of ABs especially for NGC 6397, but this is not enough to make up for the lower specific X-ray luminosity. The poor statistics in the open clusters left aside, CVs appear underrepresented in globular clusters as well, by about an order of magnitude. A likely explanation is that dynamical encounters have a net effect of destroying ABs—both those with evolved components and wider orbits and main-sequence systems—and CVs. At the same time, the correlation with encounter rate found by Pooley & Hut (2006) implies that at least CVs are formed as well; perhaps this is why the specific frequencies in open and globular clusters are less disparate for CVs than for ABs. AB-like sub-subgiants are underabundant in globular clusters as well, but on the other hand sub-subgiants in (candidate) binary MSPs are not found in open clusters (note that in Table 4 the different types of sub-subgiants are grouped together because some have not been studied well enough to make the distinction).

The relative lack of ABs in NGC 6397 with respect to other globular clusters was already noted by Bassa et al. (2004) and Grindlay (2006), who ascribed it to its post-collapsed state. We now show that 47 Tuc is deficient in ABs, too. M 4, studied by Bassa et al. (2004) and not included in Table 4, shows the same effect. Even if all fifteen sources or so that are brighter than 1×10^{30} erg s⁻¹ were ABs (which is not the case as there are also CVs, background and foreground sources, and an MSP among them), it is not enough to reach the number of ABs expected based on scaling by mass from open clusters. Milone et al. (2012) find a lower overall binary fraction in globulars compared to open clusters (Sollima et al. 2010). If this is the result of binary destruction, the X-

⁸ $\sim 15\%$ in NGC 6791, $\sim 45\%$ in M 67

⁹ Moreover, some sources seem to be missing from the list of six detected cluster members in Gondoin (2005). ROSAT source X 29 in Belloni et al. (1998), which is the brightest cluster X-ray source, is not included in the source list despite being clearly visible in the EPIC-MOS images; in the *XMM-Newton* Serendipitous Source Catalog (Watson et al. 2009) it has a maximum source detection likelihood of 279. ROSAT source X 21 is identified by Belloni et al. (1998) with a likely short-period AB and cluster member. The offset between this optical source and the corresponding *XMM-Newton* source S 17 is $3.2''$, and it is unclear why it was not identified as a potential counterpart given the match radius of $8''$ that is adopted by Gondoin (2005).

Table 4
X-ray sources in globular and old open clusters ($r \lesssim r_h$, $L_X \gtrsim 1 \times 10^{30}$ erg s $^{-1}$)

cluster	age (Gyr)	M (M_\odot)	N_X	$N_{X,CV}$	$N_{X,S}$	$N_{X,AB}$	$N_{X,AB-MS}$	$N_{X,AB-G}$	$\log(2 L_{30}/M)$
NGC 6819	2–2.4	2600	6–7	1?	1?	1?	0	1?	...
M 67	4	1100	12	0	1	7–8	5–6	2	28.9
NGC 6791	8	5000–7000	15–19	3–4	3	7–11	5–9	2	28.6–28.8
47 Tuc	11.2	1.3×10^6	~200	30[–119]	10	42[–131]	34	8	28.0
NGC 6397	13.9	2.5×10^5	15–18	11	2	0–2	0–2	0	27.7

Note. — We list the number of sources identified with cluster members (N_X), CVs ($N_{X,CV}$), sub-subgiants ($N_{X,S}$), and ABs ($N_{X,AB}$). We sub-divide the ABs into those on the main sequence ($N_{X,AB-MS}$) and evolved systems ($N_{X,AB-G}$). The numbers for NGC 6819, printed in *italics*, are especially uncertain due to the limited optical follow up. $\log(2 L_{30}/M)$ is, in log units, the ratio of the total X-ray luminosity of the N_X sources with $L_X \gtrsim 1 \times 10^{30}$ erg s $^{-1}$, to the cluster mass (M) divided by two to account for the selection of sources inside the half-mass radius. The X-ray luminosity refers to the 0.3–7 keV band and corresponds to emission from a 2 keV plasma. The horizontal line separates the open clusters from the globular clusters. References: Gosnell et al. (2012) for NGC 6819, van den Berg et al. (2004) for M 67, Bogdanov et al. (2010) and Cohn et al. (2010) for NGC 6397, Heinke et al. (2005) for 47 Tuc.

ray emitting, and thus hardest, binaries are affected as well. We cannot exclude that other factors are important. There is a trend of decreasing AB frequency with age for all clusters in Table 4 except NGC 6819.

In Verbunt (2000) it was first pointed out that the total *ROSAT* luminosity per unit mass of most globular clusters is lower than that of M 67. While M 67 may be exceptional in some ways (see Sect. 5.4), the last column of Table 4 shows that the specific X-ray luminosity of globular clusters may be lower than for open clusters in general. CVs, ABs, and sub-subgiants are all responsible for this. The X-ray emission from qLMXBs and MSPs in globular clusters, of which there are no confirmed cases in old open clusters, cannot make up for the lack of other types of faint sources. A more extensive investigation, based on a larger sample of globular clusters and old populations, is done by Heinke et al. (in preparation) to investigate the effects of age, central density, and metallicity on differences in the X-ray emissivity.

6. CONCLUSIONS

We have studied NGC 6791, which is one of the oldest open clusters known, in X-rays for the first time. Of the twenty *Chandra* sources that are identified with proper-motion cluster members, nineteen are binaries. We find a mix of CVs, ABs, and sub-subgiant binaries. With optical follow-up spectroscopy we confirm the classification of one CV in the cluster, and identify one new candidate CV. The origin of these and the other two cluster CVs is likely primordial. A comparison with the X-ray sources in the younger cluster NGC 6819 suggests that in order to find numerous (main-sequence) ABs brighter than $L_X = 1 \times 10^{30}$ erg s $^{-1}$ in open clusters, one must look at those older than ~2.5 Gyr. The mass-specific frequency of main-sequence and sub-giant ABs in NGC 6791 (8 Gyr) is 3–7 times lower than in M 67 (4 Gyr); it is not clear why this is the case. Comparison with a small number of globular clusters shows that all three source classes that are mainly responsible for the X-ray emission from old open clusters are under-represented in the globulars. This accounts for the lower total X-ray luminosity per unit mass of globular clusters, and indicates that the net effect of dynamical encounters may be destruction of—even the hardest—binaries. The cutoff luminosity for comparing source populations among clusters was set at $L_X = 1 \times 10^{30}$ erg s $^{-1}$ (0.3–7 keV). A lower cutoff luminosity might be needed to account for effects of variations of the AB X-ray luminosity function with age or metallicity. While Verbunt (2000) note that population-II ABs may have lower X-ray luminosities, it remains unclear in this context why NGC 6791, which has a super-solar metallicity, should

also have relatively fewer ABs above our limiting L_X . We defer a more thorough investigation to a future study. Deeper data are needed for NGC 6791 to match the already deep existing data for M 67, 47 Tuc, and NGC 6397. The X-ray derived AB populations may then be compared to those derived from other wavelengths, e.g. optical variability studies. Also in this respect, studies of NGC 6791 may benefit from being in the field of view of the *Kepler* satellite.

The authors would like to thank J. Hong for providing the routines to compute energy quantiles, C. Heinke for comments on the manuscript, and K. Cudworth for providing a catalog of proper motions. This research was supported by *Chandra* grant GO0-11110X. Some of the observations reported here were obtained at the MMT Observatory, a joint facility of the Smithsonian Institution and the University of Arizona.

Facilities: CXO, FLWO:1.5m (FAST), MMT (Hectospec)

REFERENCES

- Albrow, M. D., Gilliland, R. L., Brown, T. M., Edmonds, P. D., Guhathakurta, P., & Sarajedini, A. 2001, *ApJ*, 559, 1060
- Bassa, C. et al. 2004, *ApJ*, 609, 755
- Basu, S. et al. 2011, *ApJ*, 729, L10
- Bedin, L. R., Piotto, G., Carraro, G., King, I. R., & Anderson, J. 2006, *A&A*, 460, L27
- Bedin, L. R., Salaris, M., Piotto, G., Cassisi, S., Milone, A. P., Anderson, J., & King, I. R. 2008, *ApJ*, 679, L29
- Belloni, T. 1997, *Mem. Soc. Astron. Italiana*, 68, 993
- Belloni, T., Verbunt, F., & Mathieu, R. D. 1998, *A&A*, 339, 431
- Belloni, T., Verbunt, F., & Schmitt, J. H. M. M. 1993, *A&A*, 269, 175
- Bessel, M. S., Castelli, F., & Plez, B. 1998, *A&A*, 333, 231
- Bogdanov, S., van den Berg, M., Heinke, C. O., Cohn, H. N., Lugger, P. M., & Grindlay, J. E. 2010, *ApJ*, 709, 241
- Bruntt, H., Bruntt, H., Grundahl, F., Clausen, J. V., Frandsen, S., Vandenberg, D. A., & Bedin, L. R. 2011, *A&A*, 525, A2
- Brogaard, K. et al. 2012, *A&A*, 543, A106
- Broos, P., Townsley, L., Getman, K., & Bauer, F. 2002, *ACIS Extract*, An ACIS Point Source Extraction Package, Pennsylvania State University, http://www.astro.psu.edu/xray/docs/TARA/ae_users_guide.html
- Bruntt, H., Grundahl, F., Tingley, B., Frandsen, S., Stetson, P. B., & Thomsen, B. 2003, *A&A*, 410, 323
- Byckling, K., Mukai, K., Thorstensen, J. R., & Osborne, J. P. 2010, *MNRAS*, 408, 2298
- Carraro, G., Villanova, S., Demarque, P., McSwain, M. V., Piotto, G., & Bedin, L. R. 2006, *ApJ*, 643, 1151
- Cohn, H. N. et al. 2010, *ApJ*, 722, 20
- Davenport, J. R. A., & Sandquist, E. L. 2010, *ApJ*, 711, 559
- de Marchi, F. et al. 2007, *A&A*, 471, 515
- Edmonds, P. D., Gilliland, R. L., Heinke, C. O., & Grindlay, J. E. 2003a, *ApJ*, 596, 1177

- . 2003b, *ApJ*, 596, 1197
- Fan, X. et al. 1996, *AJ*, 112, 628
- Flower, P. J. 1996, *ApJ*, 469, 355
- Gänsicke, B. T. et al. 2009, *MNRAS*, 397, 2170
- Garnavich, P., Still, M., & Barclay, T. 2011, *The Astronomer's Telegram*, 3507, 1
- Geller, A. M., & Mathieu, R. D. 2012, *AJ*, 144, 54
- Giardino, G., Pillitteri, I., Favata, F., & Micela, G. 2008, *A&A*, 490, 113
- Gondoin, P. 2005, *A&A*, 438, 291
- Gosnell, N. M., Pooley, D., Geller, A. M., Kalirai, J., Mathieu, R. D., Frinchaboy, P., & Ramirez-Ruiz, E. 2012, *ApJ*, 745, 57
- Gray, R. O., & Corbally, J. C. 2009, *Stellar Spectral Classification*, ed. Gray, R. O. & Corbally, C., J. (Princeton University Press)
- Grindlay, J. et al. 2005, *ApJ*, 635, 920
- Grindlay, J. E. 2006, *Advances in Space Research*, 38, 2923
- Güdel, M. 2004, *A&A Rev.*, 12, 71
- Harrison, T. E., Johnson, J. J., McArthur, B. E., Benedict, G. F., Szkody, P., Howell, S. B., & Gelino, D. M. 2004, *AJ*, 127, 460
- Hartman, J. D., Stanek, K. Z., Gaudi, B. S., Holman, M. J., & McLeod, B. A. 2005, *AJ*, 130, 2241
- Heinke, C. O., Grindlay, J. E., Edmonds, P. D., Cohn, H. N., Lugger, P. M., Camilo, F., Bogdanov, S., & Freire, P. C. 2005, *ApJ*, 625, 796
- Heinke, C. O., Ruiter, A. J., Munro, M. P., & Belczynski, K. 2008, in *American Institute of Physics Conference Series*, Vol. 1010, *A Population Explosion: The Nature & Evolution of X-ray Binaries in Diverse Environments*, ed. R. M. Bandyopadhyay, S. Wachter, D. Gelino, & C. R. Gelino, 136–142
- Heinke, C. O., Rybicki, G. B., Narayan, R., & Grindlay, J. E. 2006, *ApJ*, 644, 1090
- Hong, J., Schlegel, E. M., & Grindlay, J. E. 2004, *ApJ*, 614, 508
- Hong, J., van den Berg, M., Schlegel, E., Grindlay, J., Koenig, X., Laycock, S., & Zhao, P. 2005, *ApJ*, 635, 907
- Hurley, J. R., Pols, O. R., Aarseth, S. J., & Tout, C. A. 2005, *MNRAS*, 363, 293
- Hut, P. 1981, *A&A*, 99, 126
- Jacoby, G. H., Hunter, D. A., & Christian, C. A. 1984, *ApJS*, 56, 257
- Kalirai, J. S. et al. 2001, *AJ*, 122, 266
- Kaluzny, J. 2003, *Acta Astronomica*, 53, 51
- Kaluzny, J., & Rucinski, S. M. 1993, *MNRAS*, 265, 34
- Kaluzny, J., Stanek, K. Z., Garnavich, P. M., & Challis, P. 1997, *ApJ*, 491, 153
- Kaluzny, J., & Udalski, A. 1992, *Acta Astronomica*, 42, 29
- Kim, M., Wilkes, B. J., Kim, D.-W., Green, P. J., Barkhouse, W. A., Lee, M. G., Silverman, J. D., & Tananbaum, H. D. 2007, *ApJ*, 659, 29
- Latham, D. W., Mathieu, R. D., Milone, A. A. E., & Davis, R. J. 1992, in *Binaries as tracers of stellar formation*, ed. A. Duquennoy & M. Mayor (Cambridge: Cambridge University Press), 132
- Liebert, J., Saffer, R. A., & Green, E. M. 1994, *AJ*, 107, 1408
- Mathieu, R. D. 2000, in *Astronomical Society of the Pacific Conference Series*, Vol. 198, *Stellar Clusters and Associations: Convection, Rotation, and Dynamos*, ed. R. Pallavicini, G. Micela, & S. Sciortino, 517–+
- Mathieu, R. D. 2008, in *IAU Symposium*, Vol. 246, *IAU Symposium*, 79–88
- Mathieu, R. D., Meibom, S., & Dolan, C. J. 2004, *ApJ*, 602, L121
- Mathieu, R. D., van den Berg, M., Torres, G., Latham, D., Verbunt, F., & Stassun, K. 2003, *AJ*, 125, 246
- Meibom, S. et al. 2009, *AJ*, 137, 5086
- Milone, A. P. et al. 2012, *A&A*, 540, A16
- Mochejska, B. J., Stanek, K. Z., & Kaluzny, J. 2003, *AJ*, 125, 3175
- Mochejska, B. J., Stanek, K. Z., Sasselov, D. D., & Szentgyorgyi, A. H. 2002, *AJ*, 123, 3460
- Mochejska, B. J. et al. 2005, *AJ*, 129, 2856
- Pallavicini, R. 1989, *A&A Rev.*, 1, 177
- Patterson, J., Thorstensen, J. R., & Knigge, C. 2008, *PASP*, 120, 510
- Perets, H. B., & Fabrycky, D. C. 2009, *ApJ*, 697, 1048
- Platais, I., Cudworth, K. M., Kozhurina-Platais, V., McLaughlin, D. E., Meibom, S., & Veillet, C. 2011, *ApJ*, 733, L1
- Pooley, D., & Hut, P. 2006, *ApJL*, 646, L143
- Predehl, P., & Schmitt, J. H. M. M. 1995, *A&A*, 293, 889
- Pretorius, M. L., & Knigge, C. 2012, *MNRAS*, 419, 1442
- Pryor, C., & Meylan, G. 1993, in *Astronomical Society of the Pacific Conference Series*, Vol. 50, *Structure and Dynamics of Globular Clusters*, ed. S. G. Djorgovski & G. Meylan, 357
- Richer, H. B., Fahlman, G. G., Rosvick, J., & Ibata, R. 1998, *ApJ*, 116, L91
- Ritter, H., & Kolb, U. 2003, *A&A*, 404, 301, (update RKcat7.18, 2012)
- Robin, A. C., Reylé, C., Derrière, S., & Picaud, S. 2003, *A&A*, 409, 523
- Rogel, A. B., Cohn, H. N., & Lugger, P. M. 2008, *ApJ*, 675, 373
- Rucinski, S. M., Kaluzny, J., & Hilditch, R. W. 1996, *MNRAS*, 282, 705
- Schlegel, D. J., Finkbeiner, D. P., & Davis, M. 1998, *ApJ*, 500, 525
- Schwope, A. D., Staude, A., Koester, D., & Vogel, J. 2007, *A&A*, 469, 1027
- Sollima, A., Carballo-Bello, J. A., Beccari, G., Ferraro, F. R., Pecci, F. F., & Lanzoni, B. 2010, *MNRAS*, 401, 577
- Stetson, P. B., Bruntt, H., & Grundahl, F. 2003, *PASP*, 115, 413
- Stoeck, J. T., Morris, S. L., Gioia, I. M., Maccacaro, T., Schild, R., Wolter, A., Fleming, T. A., & Henry, J. P. 1991, *ApJS*, 76, 813
- Thorstensen, J. R. 2003, *AJ*, 126, 3017
- Thorstensen, J. R., Lépine, S., & Shara, M. 2008, *AJ*, 136, 2107
- Tozzi, P. et al. 2006, *A&A*, 451, 457
- van den Berg, M., Orosz, J., Verbunt, F., & Stassun, K. 2001, *A&A*, 375, 375
- van den Berg, M., Tagliaferri, G., Belloni, T., & Verbunt, F. 2004, *A&A*, 418, 509
- Vanden Berk, D. E. et al. 2001, *AJ*, 122, 549
- Verbunt, F. 2000, in *Astronomical Society of the Pacific Conference Series*, Vol. 198, *Stellar Clusters and Associations: Convection, Rotation, and Dynamos*, ed. R. Pallavicini, G. Micela, & S. Sciortino, 421
- Verbunt, F., & Phinney, E. S. 1995, *A&A*, 296, 709
- Watson, M. G. et al. 2009, *A&A*, 493, 339
- Yadav, R. K. S. et al. 2008, *A&A*, 484, 609
- Zahn, J.-P. 1989, *A&A*, 220, 112